PART I

Univ. Calif

SEMIANNUAL PROGRESS REPORT

NASA RESEARCH GRANT NGL 05-007-004

FOR THE PERIOD

JANUARY 1, 1971 - June 30, 1971

N71-76336

(ACCESSION NUMBER) (THRU)

92 None

(PAGES) (CODE)

CR-123376

(NASA CR OR TMX OR AD NUMBER) (CATEGORY)

FACILITY FORM 602

DEC 1971
RECEIVED
NASA STI FACILITY
INPUT BRANCH

Table of Contents

Part I: Semiannual Progress Report

BACKGROUND INFORMATION 1

PROGRESS DURING THE REPORTING PERIOD 2

A. CHARGED PARTICLE RESEARCH 2

1. Electron Spectrometer for OGO-5 2

2. Electron Spectrometer for OGO-6 2

3. Radial Diffusion Studies 3

B. MAGNETIC FIELDS RESEARCH 4

1. Introduction 4

2. Instrument Development 4

3. Experimental Studies--ATS 1 4

4. Theoretical Studies 5

a) Solar Wind Interactions with the Interstellar Medium 5

b) Solar Wind Interaction with Venus 5

c) Solar Wind Model Studies 6

C. PROPOSALS 6

D. ASILOMAR "SOLAR WIND CONFERENCE" 7

E. STUDENT PARTICIPATION 8

F. PUBLICATIONS AND REPORTS 10

G. ABSTRACTS 15

APPENDIX A: REPORT ON THE ATS-1 MAGNETOMETER PROJECT

BACKGROUND INFORMATION

NASA research grant NGL 05-007-004 was awarded to the Institute of Geophysics and Planetary Physics of the University of California, Los Angeles, on March 1, 1962, in support of a space instrument development program. The participation of graduate students at the University is a basic part of this research effort.

The grant was renewed on July 1, 1963, with provision for a three-year step funding arrangement. Additional supplements have been provided in July 1964, July 1965, October 1966, October 1967, October 1968, October 1969, and October 1970.

The investigators whose work is supported under this grant, in the course of this work, have participated or are participating in the Mariner 2, Mariner 4, Mariner 5 projects, the OV1-2 and OV1-12 satellite projects, both USAF, the ATS 1, the OGO 5 and OGO 6 satellite projects and the Apollo 15 lunar subsatellite project. They are participating in preparations for flight experiments for the ATS's F and G, Pioneers (Jupiter) F and G, and Apollo 16. Fabrication of the flight hardware for these experiments is funded under separate contracts.

During the reporting period three new proposals were prepared by the investigators. The major portion of the proposal work was supported under this grant.

Progress During the Reporting Period

A. CHARGED PARTICLE RESEARCH

1. Electron Spectrometer for OGO-5. (PI supported in part with funds from this grant.) OGO-5 operations were terminated in October, 1971. Continuing studies are being made of various phenomena in cooperation with other experimenters on this spacecraft.

Work completed during the reporting period includes a paper on substorm particle observations which constitutes one of a series being submitted simultaneously for publication. This series presents the observations and interpretations of half a dozen OGO-5 experimenters on a particular pair of substorms. All of the observations are interpreted within the framework of a substorm model.

Also completed in the reporting period is a study of the distribution in space and time of electrons 750 kev in the geomagnetic tail. A theoretical study of electron energization in the tail is now being undertaken, stimulated by the results of the theoretical study.

2. Electron Spectrometer for OGO-6. (PI supported in part with funds from this grant.) During the reporting period a study of the correlation between chorus observations by R.E. Holzer and our energetic precipitating electrons was completed. These correlations give strong support to the Kennel-Petshek theory of strong precipitation by showing that both the waves and particles predicted by the theory are present at the same time. Additional studies with OGO-6 data include the detailed study of individual strong precipitation events, and a study of the rate of decay of electrons as a function of L during geomagnetically quiet conditions.

3. Radial Diffusion Studies. The study of high energy inner zone protons which predicts the equilibrium distribution under the mechanisms of radial diffusion, neutron decay, and atmospheric collision loss was completed during the reporting period and is now in press.

The study of inner zone electron population by inward radial diffusion during a geomagnetic storm has been completed, and the finished draft is being circulated for criticism to several scientists whose data have been used.

Underway now is an attempt to add the effect of the secular change of the earth's magnetic field to those already considered in the high-energy proton distribution problem in order to find if the agreement between the theory and the observations can be improved.

B. MAGNETIC FIELDS RESEARCH

1. Introduction. The research activities discussed in this section are directed primarily toward the study of magnetohydrodynamic phenomena in the tenuous plasma above the ionosphere and in interplanetary space. A secondary goal is the direct measurement of the magnetic fields of planetary bodies. The work includes the development of the instruments with which to obtain such measurements and in some cases the reduction and analysis of data obtained with these instruments.

2. Instrument Development. During the reporting period magnetometer development studies, particularly studies of techniques of fabrication of ring core sensors, were continued.

3. Experimental Studies--ATS 1. The UCLA magnetometer on the synchronous satellite ATS 1 has operated nearly continuously since launch in December 1966, making vector measurements of the earth's magnetic field. The high time resolution and high sensitivity of the magnetometer as well as the fixed location of the satellite have made it possible to carry out a number of unique studies.

Our ATS-1 work during the reporting period included studies of meridional field oscillations detected during geomagnetic storms, field aligned currents, and satellite-surface correlations and multiple satellite correlations.

A detailed report of our ATS-1 project is included as Appendix A.

4. Theoretical Studies.

a) Solar Wind Interactions with the Interstellar Medium. We have proposed that one effect of the ionization of interstellar neutrals in the solar wind is an unwinding of the spiralled interplanetary field. This effect is caused by a transfer of angular momentum from the electromagnetic field of the solar wind to the interstellar particles as these particles become ionized. Our preliminary calculations on this process indicate that the interplanetary magnetic field is primarily radial past the orbit of Jupiter. This possibility can be readily examined with direct observations from the magnetometers on board Pioneers F and G. However, some indirect evidence for it already exists. First, deviations from spiral angle toward values smaller than predicted were observed on the Mariner 4 flight to Mars. In addition, the cosmic ray modulation region (approximately 3-5 AU) suggests a significant change in the magnetic properties of the solar wind.

During the reporting period, a preliminary program for analyzing the transfer of angular momentum was written. It was then applied to the simple density models proposed to explain the Lyman-alpha observations of OGO 5.

b) Solar Wind Interaction with Venus. In this study, the interaction of the solar wind with Venus is as an electromagnetic coupling with the lower ionosphere and an associated mass loading of the flow in the exosphere. Such an interaction is consistent with the pressure balance requirements at the anemopause. It is also compatible with various models of the

atmospheric evolution of Venus because the net effect of the mass transfer is net loss of planetary gas. Through a theoretical relationship, the plasma mass density observed by Mariner 5 can be used as a constraint upon exospheric neutral models. Helium, in an equilibrium between solar wind loss and radiogenic production, is proposed as the dominant exospheric gas. The possibility of detecting gases lost from the planet in the solar wind was explored during the reporting period. In addition, the effect of solar wind induced loss upon atmospheric evolution was investigated. Preliminary results indicate that atmospheric helium as He^+ can be detected downstream from the planet and that solar wind induced loss from Venus is not an important process unless the solar wind mass flux was several orders of magnitude greater in the geological past.

c) Solar Wind Model Studies. During the reporting period we continued work on models of the solar wind which include magnetic and rotational effects. Using a first order expansion of the magnetohydrodynamic equations about the non-rotating Parker solution, we developed approximations that reduced the machine time required to run the problem. Results to date indicate a latitudinal flow velocity and associated latitudinal component of the interplanetary magnetic field which has not been considered in earlier models of the solar wind.

C. PROPOSALS

During the reporting period three new proposals were produced by the group supported under this grant. The first proposal was

for a study of the heliographic latitude dependence of the interplanetary magnetic field using simultaneous measurements from several satellites and space probes. The second was for the qualification testing of the Apollo 15 lunar subsatellite magnetometer instruments. The last was for a magnetic field experiment for the Grand Tour Missions to the Outer Planets.

We have been selected for the definition phase of the Grand Tour mission and have been funded to carry out the magnetic fields investigation study.

D. ASILOMAR "SOLAR WIND CONFERENCE"

During the reporting period some of the investigators participated in the organization and operation of the Asilomar "Solar Wind Conference" sponsored by the University of California (Berkeley and Los Angeles) and the NASA Ames Research Center. This conference work was supported in part by funds from this grant.

E. STUDENT PARTICIPATION

A basic purpose of our research is to make it possible for students to participate in scientific experiments within the rapidly developing field of space science. The following graduate students have participated in our programs during the period covered by this report.

1. Carlene Arthur, Department of Planetary and Space Science, is studying the physics of the magnetosphere.

2. Joseph Barfield, Department of Planetary and Space Science, is studying the physics of the magnetosphere and the interplanetary medium.

3. Mac C. Chapman, Department of Planetary and Space Science, is working on the strong precipitation data obtained from the electron spectrometer on OGO-6.

4. Donald Childers, Department of Physics, is studying the physics of the magnetosphere. He is working with data from OGO-5 and ATS-1.

5. Bryan Horning, Department of Planetary and Space Science, is studying the physics of the magnetosphere.

6. Lawrence Sharp, Department of Planetary and Space Science, is concentrating on the development of spacecraft magnetometers.

7. Albert Tomassian, Department of Planetary and Space Science, is studying the trapped radiation in the earth's magnetosphere. During the reporting period Mr. Tomassian completed the requirements for the Ph.D. in Planetary and Space Physics. His dissertation was a study of radial diffusion as a transport mechanism

for the electrons of the inner zone.

8. The work of Ray Walker, Department of Planetary and Space Science, involves the study of electrons in the magnetotail, using data from the electron spectrometer on OGO-5.

9. C.R. Winge, Jr., Department of Planetary and Space Science, is developing models of the solar expansion which include the effects of electromagnetic forces and solar rotation. During the reporting period Mr. Winge completed the requirements for the Ph.D. in Planetary and Space Physics. His dissertation is entitled "Latitude Effects in the Solar Wind".

10. Edwin Winter, Department of Planetary and Space Science, is studying the interaction of the solar wind with planetary and cometary bodies and the termination of the solar wind.

All of the registered graduate students whose support is provided by these programs are employed as research assistants in classifications normally open to graduate students under long-established UCLA regulations. Their rates of pay are established by the Regents of the University. A considerable effort is made to assign research tasks which are of special interest to the student, but the tasks themselves are not necessarily related directly or indirectly to any dissertation research that the student may eventually perform.

F. PUBLICATIONS AND REPORTS

Papers resulting, wholly or in part, from the research supported under this grant are listed chronologically below. An asterisk denotes a paper completed since the last report.

Coleman, P.J., Jr., L. Davis, Jr., E.J. Smith, and C.P. Sonett, Interplanetary magnetic fields: Preliminary Observations from Mariner II, Science, 138, 1099, 1962.

Farley, T.A., The growth of our knowledge of the earth's outer radiation belt, Rev. Geophys., 1, 3, 1963.

Smith, E.J., L. Davis, Jr., P.J. Coleman, Jr., and C.P. Sonett, Magnetic fields measured in the vicinity of Venus: Preliminary observations from Mariner II, Science, 139, 909, 1963.

Coleman, P.J., Jr., Characteristics of the region of interaction between the interplanetary plasma and the geomagnetic field: Pioneer 5, J. Geophys. Res., 69, 3051, 1964.

Smith, E.J., L. Davis, Jr., P.J. Coleman, Jr., and C.P. Sonett, Interplanetary magnetic field measurements: The Mariner II magnetometer experiment, in The Solar Wind, edited by R.C. Mackin and M.M. Neugebauer, Pergamon Press, New York, 1966.

Sonett, C.P., D.S. Colburn, L. Davis, Jr., E.J. Smith, and P.J. Coleman, Jr., Evidence for a collision-free magnetohydrodynamic shock in interplanetary space, Phys. Rev. Letters, 13, 153, 1964.

Smith, E.J., L. Davis, Jr., P.J. Coleman, Jr., and C.P. Sonett, Magnetic measurements near Venus, J. Geophys. Res., 70, 7, 1964.

Coleman, P.J., Jr., The Mariner-2 magnetometer experiment and associated data reduction procedures, Publication No. 447, Institute of Geophysics and Planetary Physics, University of California, Los Angeles, May, 1965.

Farley, T.A., Space Sciences, VI, NASA Document No. SP-114, Washington, D.C., 1966.

Coleman, P.J.,Jr., E.J. Smith, L. Davis, Jr., and D.E. Jones, Measurements of magnetic fields in the vicinity of the magnetosphere and in interplanetary space: Preliminary results from Mariner 4, in Space Research VI, edited by R.L. Smith-Rose, Spartan Books, Washington, D.C., 1966.

Smith, E.J., L. Davis, Jr., P.J. Coleman, Jr., and D.E. Jones, Magnetic field measurements near Mars: Mariner 4 preliminary report, Science, 149, 1241, 1965.

Coleman, P.J., Jr., Irregularities in the interplanetary magnetic field, Publication No. 467, Institute of Geophysics and Planetary Physics, University of California, Los Angeles, 1965.

Coleman, P.J., Jr., Interaction of the solar wind with the planets, AIAA Journal, 4, 4-9, 1965.

Coleman, P.J., Jr., L. Davis, Jr., E.J. Smith, and D.E. Jones, Variations in the polarity distribution of the interplanetary magnetic field, J. Geophys. Res., 71, 2831-2839, 1966.

Coleman, P.J., Jr., Hydromagnetic waves in the interplanetary plasma, Phys. Rev. Letters, 17, 207-211, 1966.

Coleman, P.J., Jr., Variations in the interplanetary magnetic field: Mariner 2, 1, Observed properties, J. Geophys. Res., 71, 5509-5531, 1966.

Coleman, P.J., Jr., and E.J. Smith, An interpretation of the subsidiary peaks at periods near 27 days in the power spectra of Ci and Kp, J. Geophys. Res., 71, 4685, 1966.

Snare, R.C., and C.R. Benjamin, A magnetic field instrument for the OGO-E spacecraft, IEEE Trans. Nuc. Sci., NS-13, 333-339, 1966.

Barry, J.D., and R.C. Snare, A fluxgate magnetometer for the Applications Technology Satellite, IEEE Trans. Nuc. Sci., NS-13, 326-331, 1966.

Siscoe, G.L., L. Davis, Jr., E.J. Smith, P.J. Coleman, Jr., and D.E. Jones, Magnetic fluctuations in the magnetosheath: Mariner 4, J. Geophys. Res., 72, 1-17, 1967.

Coleman, P.J., Jr., L. Davis, Jr., E.J. Smith, and D.E. Jones, The polarity pattern of the interplanetary magnetic field during solar rotations 1798-1808, J. Geophys. Res., 72, 1637-1643, 1967.

Coleman, P.J., Jr., Wave-like phenomena in the interplanetary plasma: Mariner 2, Planet. Space Sci., 15, 953, 1967.

Coleman, P.J., Jr., Variations in the interplanetary magnetic field and some effects upon solar cosmic rays, Planet. Space Sci., 15, 975-995, 1967.

Ballif, J.R., D.E. Jones, P.J. Coleman, Jr., L. Davis, Jr., and E.J. Smith, Transverse fluctuations in the interplanetary magnetic field: A requisite for geomagnetic variability, J. Geophys. Res., 72, 4357-4364, 1967.

Coleman, P.J., Jr., On the excitation of the magnetosphere by the solar wind, J. Geophys. Res., 72, 5518, 1967.

Barry, J.D., P.J. Coleman, Jr., W.F. Libby, and L.M. Libby, Radio reflection by free radicals in the earth's atmosphere, Science, 156, 1730-1732, 1967.

Snare, R.C., and G.N. Spellman, Digital offset field generator for spacecraft magnetometers, Publication No. 618, Institute of Geophysics and Planetary Physics, University of California, Los Angeles, 1967.

Barry, J.D., and L.L. Simmons, A heater for a fluxgate magnetometer sensor on the fifth Orbiting Geophysical Observatory satellite, IEEE Conf. IGA, 34C62, 1967.

Farley, T.A., Van Allen radiation belts, in The Encyclopedia of Atmospheric Sciences and Astrogeology, edited by R.W. Fairbridge, 1075-1083, Reinhold Publishing Co., New York, 1967.

Schubert, G., and P.J. Coleman, Jr., The angular momentum of the solar wind, Ap. J., 153, 943-950, 1968.

Coleman, P.J., Jr., Turbulence, viscosity, and dissipation in the solar wind plasma, Ap. J., 153, 371-388, 1968.

Winge, C.R., Jr., and P.J. Coleman, Jr., The motion of charged particles in a spiral field, J. Geophys. Res., 73, 165-173, 1968.

Chapman, M.C., and T.A. Farley, Absolute electron fluxes and energies in the inner radiation zone in 1965, J. Geophys. Res., 73, 6825-6833, 1968.

Farley, T.A., Radial diffusion of electrons at low L values, J. Geophys. Res., 74, 377-380, 1969.

Intriligator, D.S., Albedo neutron source for high-energy protons trapped in the geomagnetic field, Phys. Rev. Letters, 20, 1048-1049, 1968.

Farley, T.A., A.D. Tomassian, and M.C. Chapman, Evaluation of CRAND source for 10 to 50 Mev trapped protons, J. Geophys. Res., 74, 4721-4730, 1969.

Farley, T.A., Radial diffusion of starfish electrons, J. Geophys. Res., 74, 3591-3600, 1969.

Cummings, W.D., P.J. Coleman, Jr., and G.L. Siscoe, The quiet day magnetic field at ATS 1, J. Geophys. Res., in press, 1971.

Coleman, P.J., Jr., and W.D. Cummings, The storm-time disturbance field at ATS 1, J. Geophys. Res., 76, (1), 51-62, 1971.

Barfield, J.N., and P.J. Coleman, Jr., Storm-related wave phenomena observed at the synchronous, equatorial orbit, J. Geophys. Res., 75, 1943-1946, 1970.

Coleman, P.J., Jr., and R.L. McPherron, Fluctuations in the distant geomagnetic field during substorms: ATS 1, in Particles and Fields in the Magnetosphere, edited by B.M. McCormac, D. Reidel Publ. Co., Dordrecht, Holland, 1970.

Coleman, P.J., Jr., Magnetic field pulsations at ATS 1, Ann. Geophys., 26, (3), 719-734, 1970.

Coleman, P.J., Jr., Geomagnetic storms at ATS 1, in Intercorrelated Satellite Observations Related to Solar Events, edited by V. Manno and D.E. Page, D. Reidel Publ. Co., Dordrecht, Holland, 1970.

McPherron, R.L., and P.J. Coleman, Jr., Magnetic fluctuations during magnetospheric substorms, J. Geophys. Res., 75, 3927-3931, 1970.

Patel, V.L., and P.J. Coleman, Jr., Sudden impulses in the magnetosphere observed at synchronous orbit, J. Geophys. Res., 75, (34), 7255-7260, 1970.

McPherron, R.L., C.T. Russell, and P.J. Coleman, Jr., Comparison of the Olson field model to quiet day magnetic field observations at ATS 1, Proc. Conf. Quantitative Magnetospheric Models, Boulder, Colorado, 1970.

McPherron, R.L., The growth phase of magnetospheric substorms, J. Geophys. Res., 75, (28), 5592-5599, 1970.

Farley, T.A., A.D. Tomassian, and M. Walt, Source of high-energy protons in the Van Allen radiation belt, Phys. Rev. Letters, 25, 47-49, 1970.

Russell, C.T., R.L. McPherron, and P.J. Coleman, Jr., Magnetic field variations in the near geomagnetic tail associated with weak substorm activity, J. Geophys. Res., 76 (7), 1823-1829, 1971.

*Winge, C.R., Jr., and P.J. Coleman, Jr., Magnetic latitude effects in the solar wind, to appear in the Proceedings of the Asilomar Conference on the Solar Wind, 1971.

*Coleman, P.J., Jr., and E.M. Winter, Effects of interstellar particles upon the interplanetary magnetic field, to appear in the Proceedings of the Asilomar Conference on the Solar Wind, 1971

*McPherron, R.L., and P.J. Coleman, Jr., Satellite observations of band-limited micropulsations during a magnetospheric substorm, J. Geophys. Res., 76 (13), 3010-3021, 1971.

*Barfield, J.N., L.J. Lanzerotti, C.G. Maclennan, G.A. Paulikas, and M. Schulz, Quiet-time observation of a coherent compressional Pc 4 micropulsation at synchronous altitude, submitted to J. Geophys. Res., 1971.

*Farley, T.A. and M. Walt, The source and loss processes of inner radiation belt protons, accepted by J. Geophys. Res., 1971.

*Walt, M. and T.A. Farley, High energy proton model for the inner radiation belt, presented at Summer Advanced Institute on Earth's Particles and Fields, Cortina, Italy, 1971.

*Tomassian, A.D. and T.A. Farley, Inner zone energetic electron repopulation by radial diffusion, submitted to J. Geophys. Res., 1971.

G. ABSTRACTS

Abstracts of papers and talks concerning results of the research performed, wholly or in part, under this grant are included in this section. These abstracts pertain to papers completed during the reporting period and to talks prepared during this period.

Satellite Observations of Band-Limited Micropulsations during a Magnetospheric Substorm

R.L. McPherron and P.J. Coleman, Jr.
Department of Planetary and Space Science and
Institute of Geophysics and Planetary Physics
University of California, Los Angeles 90024

Band limited micropulsations have been observed in space by the UCLA fluxgate magnetometer on OGO 5. Throughout the event the satellite was inbound on the dawn meridian between 7 and 5 R_E just below the magnetic equatorial plane. These pulsations were quasi-sinusoidal, with period 20 sec and rms amplitude of 0.3γ. Their average polarization was transverse to the main magnetic field, with the major axis azimuthal in the equatorial plane. The average ellipticity was 0.3 and the predominant sense of rotation was right-handed with respect to the main magnetic field. Instantaneously these parameters were quite variable, with the pulsations occurring in bursts propagating at various angles to the field. During the pulsation event the main field was essentially dipolar; however, the waves were first observed just inside a sharp transition from a region in which the field magnitude had been constant for several earth radii. No modulation of trapped electrons (E>50 kev) by the pulsations greater than 4% was observed on the same satellite; however, whistler chorus did appear to consist of quasiperiodic bursts. Simultaneous magnetic field observations in the auroral zone near the subsatellite point showed that the pulsations were present there with comparable period and amplitude. Furthermore the ground data reveal that the event occurred in the last phase

of a negative bay, i.e., during the recovery phase of a magnetospheric substorm. The characteristics of the pulsations observed in space are similar to the characteristics of Pi 1 micropulsations observed on the ground during substorms and lead to identification of these as the same phenomenon. However, a comparison of the characteristics with the predictions of a recent theoretical model purporting to explain the ground observations finds the model seriously deficient.

J. Geophys. Res., 76 (13), 3010, 1971.

Effects of Interstellar Particles upon the Interplanetary Magnetic Field

P.J. Coleman, Jr. and E.M. Winter
University of California, Los Angeles

The flow of interstellar neutral particles into the interplanetary medium and their subsequent ionization in the presence of the electromagnetic field of the solar wind can cause a loss of field angular momentum by the solar wind. The effect of this loss of field momentum is a significant unwinding of the spiral field. This angular momentum effect is evaluated for a simple model of neutral density and ion production. It is found that for neutral hydrogen densities of 1 atom cm^{-3} with a relative velocity of 10-20 $km\text{-}sec^{-1}$, the spiral angle will return to 45° before the orbit of Jupiter.

To appear in the Proceedings of the Asilomar Conference on the Solar Wind, 1971.

Magnetic Latitude Effects in the Solar Wind

C.R. Winge, Jr. and P.J. Coleman, Jr.
University of California, Los Angeles

The Weber-Davis model of the solar wind is generalized to include the effects of latitude. The principal assumptions of high electrical conductivity, rotational symmetry, the polytropic relation between pressure and density, and a flow aligned field in a system rotating with the sun, are retained. An approximate solution to the resulting equations for spherical boundary conditions at the base of the corona indicates a small component of latitudinal flow toward the solar poles at large distances from the sun as a result of latitudinal magnetic forces.

To appear in the Proceedings of the Asilomar Conference on the Solar Wind, 1971.

Correlations Between Magnetic Field Changes at ATS-1 and Low Latitude Ground Stations

B.L. Horning, R.L. McPherron, and P.J. Coleman, Jr.
University of California, Los Angeles

The horizontal components of the magnetic fields measured at the synchronous satellite ATS-1, and at Honolulu and Tucson are often observed to be highly correlated. The highest correlation is present during the onset of magnetospheric substorms occurring within three hours of local midnight, and after periods of little or no disturbance from the quiet day magnetic field. A linear regression of data from Tucson, Honolulu, and Guam versus the satellite shows that the correlation depends upon local time, the magnitude of the field, and the longitudinal distribution of the ground stations. It is suggested that the phenomena responsible for these correlations are spatial and temporal changes in the tail current caused by increased magnetic pressure on the plasma sheet. Other current systems tend to destroy the correlation. The correlation may also be weakened when ATS 1 is engulfed by the tail current. We believe that this phenomenon can be used as an effective tool in studying the tail current in the absence of magnetic storms.

Presented at the Spring Meeting of the American Geophysical Union, Washington, D.C., April, 1971.

Low Frequency Waves at ATS-1 and its Conjugate Point During Substorms

R.L. McPherron, and P.J. Coleman, Jr.
University of California, Los Angeles

A geomagnetic observatory at the calculated conjugate point of the synchronous satellite ATS-1 has been used to digitally record low frequency waves during substorms. Simultaneous observations at ATS-1 reveal whether these waves are present on the field line passing through the satellite. The comparison between the two locations is made quantitative by spectral analysis of the waveform data. When a single wave phenomenon appears to be present at both locations, a transfer function for the field line is determined. Among the ground wave phenomena considered are sweepers (IPDP), noise bursts (Pi 2), irregular fluctuations and band limited pulsations (Pi 1). Not all of these are simultaneously observed at both locations indicating either the waves are localized in space with the satellite on a different field or the waves originate in the ionosphere.

Presented at the Spring Meeting of the American Geophysical Union, Washington, D.C., April, 1971.

Pc 4 and Pc 5 Micropulsations Observed During Geomagnetic Storms: ATS-1

J.N. Barfield, R.L. McPherron, and P.J. Coleman, Jr.
University of California, Los Angeles

Quasi-sinusoidal fluctuations of relatively large amplitudes are regularly observed at the ATS-1 orbit during geomagnetic storms. During the year 1967, 26 clearly defined events were observed, with periods in the range 2-15 minutes and amplitudes up to 20γ. These oscillations were usually elliptically polarized with the major axis of the polarization ellipse lying in a swept back meridional plane. The events typically occurred during the main phase of the geomagnetic storm, and were generally confined to the afternoon sector. All 26 events were closely correlated with substorm activity in the midnight sector.

Presented at the Spring Meeting of the American Geophysical Union, Washington, D.C., April, 1971.

A Modular Approach to the Digital Analysis of Vector Time Series

R.L. McPherron, and P.J. Coleman, Jr.
University of California, Los Angeles, USA

Recent investigations of such phenomena as low frequency electromagnetic waves have benefited greatly from the conveniences of digital data. The primary advantage is the wide variety of analysis techniques available through computer processing. Despite the apparent conceptual simplicity of many of these techniques, they have often proven difficult to implement. A major problem has been that simple changes in data format or analysis technique cause long delays in reprogramming of the computer. We have attempted to overcome these problems by a modular approach to time series analysis. This approach utilizes the structure of FORTRAN programming creating subroutines for each of many possible operations on time series. To facilitate internal manipulation of data we require all time series have the same format. To interface with actual input data streams we write input conversion routines as the need arises. To avoid problems in manipulation of large program decks all programs are stored internally in the direct access memory of an IBM 360-91. Access to these programs is particularly convenient because of the facilities for data set manipulation available in the operating system of this computer. The entire process of interaction with the computer is enhanced by use of a remote television console and keyboard. We will demonstrate the structure and use of this modular approach by outlining the procedure followed in the analysis of a low frequency electromagnetic wave recorded simultaneously at the synchronous

satellite ATS-1 and its auroral zone conjugate point, Tungsten, N.W.T., Canada. Instrumentation and data processing at the ground station are described in a companion paper. Particular emphasis will be placed on describing the development of a new technique for dynamic spectral analysis using the full 3 x 3 spectral matrix. This technique enables the investigator to observe a wave in an arbitrary coordinate system and determine all relevant polarization parameters as a function of frequency and time.

Presented at the XV General Assembly of the I.U.G.G., Moscow, August, 1971.

Substorm Related Changes in the Geomagnetic Tail

R.L. McPherron
University of California, Los Angeles

Changes in the configuration of the geomagnetic tail are known to play a fundamental role in magnetospheric substorms. Observations with the UCLA magnetometer on the eccentric orbiter OGO 5 indicate that the most pronounced changes in the midnight meridian occur in the cusp between 8 and 13 R_e. In order to organize the observations it is necessary to separate effects on the tail due to the solar wind magnetic field and effects due to substorms. Provided there are no changes in the solar wind there are two distinct phases of a substorm in the near tail: a growth phase and an expansion phase. During each phase the observations depend on the location of the satellite relative to the plasma sheet boundaries, far behind the earth is the pure tail region which consists of the lobe and the plasma sheet. In the lobe the field magnitude is characteristically enhanced relative to the dipole. Closer to the earth is a region of transition. The field magnitude is close to that of the dipole but its orientation is distorted forming a cusp-like field line. Near the earth is a region of depressed field. Here the field magnitude is much less that that of the dipole, but its orientation is similar. The growth phase of a substorm appears to be the direct consequence of the onset of a southward solar wind magnetic field. In the pure tail region the lobe field begins to increase in magnitude and the plasma sheet thins. The transition region moves earthward

and the field lines become more tail-like as the field magnitude increases. In the inner region of depressed field the field magnitude decreases rapidly. The onset of the expansion phase appears to be a process internal to the magnetosphere and independent of the solar wind. In the depressed field region there is a rapid, turbulent increase in field magnitude. In the transition region there is a sudden decrease in field magnitude and a return to dipolar orientation. In the tail region the plasma sheet expands rapidly with the field becoming quite dipolar inside and decreasing slowly in the lobe of the tail.

Presented at the XV General Assembly of the I.U.G.G., Moscow, August, 1971.

Substorm Wave Phenomena

R.L. McPherron
University of California, Los Angeles

In principle, low frequency waves (ULF) should provide a useful tool for studying the characteristics of magnetospheric plasma. They should be particularly useful during magnetospheric substorms when rapid changes make it difficult to interpret observations made with a single satellite. Ground observations of magnetic micropulsations have revealed that a number of distinct wave phenomena occur during substorms. At the dusk meridian IPDP (sweeper) events are associated with the expansion phase; near midnight Pi 2 (noise bursts) are associated with the growth phase and irregular pulsations with the expansion phase; post midnight Pi 1 (band limited pulsations) are associated with the recovery phase. Speculation about plasma characteristics responsible for these wave phenomena include: cyclotron instability of injected protons for IPDP, field aligned current instability for Pi 2, turbulent inward flow of magnetospheric plasma for irregular pulsations, and drift wave instability of inner edge of electron plasma sheet for Pi 1. Satellite observations of ULF waves are few in number but exceedingly important in defining characteristics not accessible to ground observations. Recent results obtained by UCLA magnetometers on ATS 1 and at its conjugate point, Tungsten, NWT, Canada, reveal the presence of each of these wave phenomena in space on auroral zone field lines. This paper will present the characteristics of these waves as derived from simultaneous observations on the ground and in space. Implications of these ob-

servations with regard to the generation of waves and their role in the substorm process will be discussed.

Presented at the XV General Assembly of the I.U.G.G., Moscow, August, 1971.

Digital Data Acquisition and Processing from a Remote Magnetic Observatory

R.C. Snare, D.J. Peters, P.J. Coleman, Jr., and R.L. McPherron
Institute of Geophysics, University of California
Los Angeles, California, USA

High quality magnetic field measurements in the auroral zone are particularly important in present studies of magnetospheric physics. The standard analog magnetometers are inappropriate because of limited dynamic range, sensitivity, and time resolution and in conveniences in the manipulation of the data. Remote observatories using satellite type magnetometers and digital data acquisition systems are therefore a desirable improvement. To complement the UCLA magnetometer on ATS-1 conjugate point at Tungsten, N.W.T., Canada. The maintainence of this station and computer processing of the data have involved a number of unexpected problems which could delay similar efforts elsewhere. Therefore, the instrumentation and data processing for this observatory will be described, with particular emphasis on outstanding problems. The advantages of this system are illustrated in a companion paper by examples of scientific results obtained using computer time series analysis. Alternatives to the use of digital incremental tape recorders as in the present system, e.g., data transmission via satellite link, will also be discussed.

Presented at the XV General Assembly of the I.U.G.G., Moscow, August, 1971.

Quiet-Time Observation of a Coherent Compressional Pc-4 Micropulsation at Synchronous Altitude

J.N. Barfield
University of California, Los Angeles

L.J. Lanzerotti and C.G. Maclennan
Bell Telephone Laboratories, Murray Hill, N.J.

G.A. Paulikas and Michael Schulz
The Aerospace Corporation, El Segundo, Calif.

During a magnetically quiet interval (1740-1850 UT), on February 14, 1967, the magnetic-field intensity and energetic electron fluxes ($E \simeq 0.3$-2.0 MeV) at ATS 1 exhibited coherent modulations having a frequency of 33.8 cph (period $\simeq$ 106.5 sec) and a duration of approximately 40 oscillations. The electron fluxes and the magnetic field oscillated in phase. The field perturbation reached 8γ (peak to peak) in the direction of the unperturbed geomagnetic field. The transverse component of the field perturbation was practically zero. The characteristics of the observed oscillations appear compatible with those of a compressional (magnetosonic) excitation of the outer magnetosphere. The substantially radial normal mode is perhaps driven by a bounce-resonant interaction with the 15-keV protons that populate the quiet-time ring current.

Submitted to J. Geophys. Res., 1971.

An Attempt at Reconciliation of Empirically Determined Radial Diffusion Coefficients

Thomas A. Farley
University of California, Los Angeles

Published values for the radial diffusion coefficient applicable to the transport of various energetic particle populations of the radiation belt show large discrepancies. An attempt is made to reconcile these discrepancies by considering the functional dependence of the coefficient on L, and on the particle drift period and pitch angle, using diffusion theory as a guide. A reasonably successful result is obtained, particularly at low L values, if the radial diffusion coefficient is assumed to be proportional to the particle drift period (which, for non-relativistic particles, implies an inverse proportion to the particle magnetic moment), and if the coefficient varies with particle pitch angle in the way computed by Falthammar for diffusion produced by magnetic variations. There remains a discrepancy among various reported values of a factor of 30 in the L range 3-5. This discrepancy is so large that it should be possible to resolve it, even with the limitations of present data sets.

Presented at the Spring Meeting of the American Geophysical Union, Washington, D.C., April, 1971.

APPENDIX A

REPORT ON THE ATS-1 MAGNETOMETER PROJECT

Table of Contents

I. INTRODUCTION A-1

1. Value of ATS-1 Data A-1
2. Problems of Spacecraft Field A-1

II. ATS-1 CHRONOLOGY A-3

III. CORRECTION OF ATS-1 MAGNETIC FIELD OBSERVATIONS A-3

1. Absolute Correction of Eclipse State A-3
   A. Sources of DC Interference A-3
   B. Determination of Perpendicular Offset in the Eclipse State A-5
   C. Determination of Parallel Offsets in the Eclipse State A-7
   D. Absolute Correction for Three Equinoxes A-7
2. Spacecraft State and Associated Correction A-8
   A. Determination of Spacecraft State A-8
   B. Determination of Relative Offsets A-11
   C. Determination of Most Frequent States A-13
   D. Determination of Absolute Correction Vectors for Most Frequent States A-14
3. Automatic Correction of Magnetometer Data A-15
   A. Correction Procedure A-15
4. Remaining Problems A-18

IV. CALCULATION OF POWER SPECTRA USING DATA WITH VARIOUS TYPES OF INTERFERENCE A-19

1. Types of Interference A-19
2. Techniques of Spectral Analysis A-22
3. Example Spectra A-25

V. SCIENTIFIC RESULTS A-27

1. Stormtime Meridional Oscillations A-27
2. Ground-Satellite Correlations A-34
   A. Transfer Function of the Field Line for Pc 1 A-34
   B. Polarization of Pc 1 in Space A-35
   C. Pi 2 Noise Bursts on the Ground and in Space A-36
   D. Band-Limited Pi 1 Micropulsations A-38
3. Support of Other Projects A-41
   A. Field Aligned Currents A-41
   B. Multi-Satellite Correlations A-42

I. INTRODUCTION

Values of ATS 1 Data. The ATS 1 satellite was placed in synchronous orbit in December 1966. Since its launch, it has operated almost continuously, measuring the vector magnetic field. At the time of launch this instrument was the most sensitive fluxgate magnetometer in space and, in addition, had the highest sample rate of any satellite magnetometer. The fact that it is located in the equatorial plane and its orbital period is locked to the rotation period of the earth has made possible a number of unique studies. All of these depend on the fact that the satellite sweeps out one complete revolution of the magnetosphere every day at a fixed point in the earth's magnetic field. This makes possible statistical studies of the occurrence of various phenomena which take place at the synchronous orbit. Any eccentric satellite requires a full year to make such a circuit and requires many years to acquire comparable statistics.

The value of such studies is enhanced by the fact that magnetic field lines intersecting the auroral zone pass near or through the synchronous orbit. This fact has made the ATS 1 data extremely useful in studies of the magnetospheric substorm, magnetic storms and auroral zone micropulsations.

Problems of Spacecraft Field. Despite the fact that the magnetometer has worked properly enabling us to complete a number of important studies, we have encountered major problems in the analysis of the data. These problems arise from the facts that the spacecraft was not originally designed to carry a magnetometer and that no boom was provided to separate the instrument from the spacecraft.

As a consequence, the spacecraft field at the magnetometer is comparable to the ambient field. This problem would not be serious if the field were known or constant. Unfortunately, this field is dependent on the spacecraft state, which changes as often as 100 times per day. Unless this field is determined for each state, no absolute measurements of the field are possible.

In addition to the problem just discussed, the absence of a boom has made it difficult to study fluctuations of the field. Here the problem arises from field transients caused by the changing spacecraft state. These transients introduce noise spikes and gaps into the magnetometer data. Similarly, other environmental experiments produce periodic disturbances at the spacecraft.

During the past year we have developed methods for handling the preceding difficulties. Use of these methods has enabled us to begin a number of interesting projects otherwise not possible. In the following sections we describe these methods and summarize the results of our analysis.

II. ATS 1 CHRONOLOGY

The UCLA magnetometer on ATS 1 has operated continuously now for almost 5 years. During this time the percent data recovered from the satellite has typically been about 80%. A month-by-month plot of this data recovery is included as Figure 1. During this time there have been two major changes in the satellite which, in order to compensate for, our existing data processing programs must be modified. The first of these occurred on November 2, 1969, when the satellite sun sensor failed. The signal from such a sensor is required to resolve the output of the magnetometer transverse to the spin axis into two orthogonal components fixed in inertial space.

The second event occurred on June 30, 1970, when Goddard Space Flight Center ceased recording the output of the EME package on ATS 1. Special arrangements made with NOAA at Boulder, Colorado, supported by the Office of Naval Research, have made it possible to continue recording the telemetered data. However, the format of the data tapes is quite different from those originally supplied to UCLA. These events and several others of lesser importance are summarized in the chronology of Table 1.

III. CORRECTION OF ATS-1 MAGNETIC FIELD OBSERVATIONS

Absolute Correction for Eclipse State

Sources of DC Interference. As viewed by our data processing program, the ATS 1 magnetometer consists of two sensors, one parallel and one perpendicular to the satellite spin axis. The parallel sensor is effectively fixed in relation to all electrical currents flowing in the rotating spacecraft and measures

the magnetic field of these currents. This spacecraft field is superimposed on the natural field parallel to the spin axis and must be subtracted from the measurements to obtain the natural field.

The perpendicular sensor rotates at the satellite spin frequency and records the projection of the transverse component of the field on the instantaneous position of the sensor. This projection is a maximum when the sensor and transverse field are parallel, and a minimum when they are antiparallel. By noting the phase of this signal relative to a signal from the sun sensor, it is possible to resolve the sensor signal into two orthogonal components.

Interference with the perpendicular sensor is caused by any magnetic field which is periodic at the spin frequency. Such a signal arises from the solar panels in two different ways. First, the magnetometer is located on the rim of a cylindrical spacecraft and during one rotation moves first toward the subsolar point and then away. Since the currents flow only in the cells near the subsolar point, the magnetometer is moving first toward the currents and then away. The magnetic field at the magnetometer due to these currents will thus increase and decrease periodically at the spin frequency. We note at a fixed point in space, there would be no variation in the magnetic field due to this effect.

There is a second way, however, in which the field varies periodically at both the magnetometer and also at a fixed point in space. This results from the asymmetric distribution of solar cells due to openings in the side of the spacecraft. Since there

are no cells, there is no current. Thus, the magnitude of the currents at the subsolar point, and hence magnetic fields at the magnetometer, are modulated periodically at the spin rate.

The above periodic variations in the magnetic field at the spin frequency are superimposed on the variation due to rotation of the perpendicular sensor in the transverse natural field. The output of this sensor is the sum of these two signals. We note also that the solar cell currents remain constant in amplitude and phase for a given state of the spacecraft. Thus, when the sensor signal is resolved into two orthogonal components, the periodic interference signal appears as constant offsets in the two orthogonal components of the transverse field. As with the parallel sensor discussed previously, these two offsets must be subtracted from the measured field to obtain the actual field.

It should be mentioned that the parallel sensor also records a signal at the spin frequency due to the above sources. Since the desired information about the natural field is at frequencies less than the spin frequency, this interference can be eliminated by low-pass filtering the output of the parallel sensor. We note, however, that for a given state of a spacecraft the phase of this interference signal depends on the relative position of the sun and the magnetometer, i.e., this error signal acts as a sun sensor.

Determination of Perpendicular Offset in the Eclipse State. For the sake of argument, let us assume that the spacecraft state remains constant. Then the offsets in the two components of the transverse field are determined as follows. Near the equinoxes a satellite in equatorial orbit is eclipsed by the earth near

local midnight. When the satellite enters the earth's shadow, the currents in the solar cells vanish along with their magnetic effects. At this time, the measured field becomes equal to the natural field. The offsets which occur in the two orthogonal components of the transverse field at this time are just the corrections which must be applied for this spacecraft state.

The actual determination of these two offsets is complicated by two factors. First, as soon as the spacecraft enters the earth's shadow the signal from the sun sensor disappears. This means that resolution of the signal from the transverse magnetometer into two orthogonal components fixed in inertial space depends upon extrapolation of the phase angle of the spacecraft's spin. This extrapolation can be made by assuming the spin rate is constant with a value equal to that at the beginning of eclipse. This assumption is valid only for a short interval of time.

The second factor is that the spacecraft begins to cool in the shadow and shrinks. This, in turn, causes it to spin faster. As a consequence, the phase angle of the spinning spacecraft differs from the predicted, and inertial reference is lost. At this point, large sinusoids appear in the X and Y components until a sun sensor signal is again available. The offsets must be measured as soon after the spacecraft enters the complete shadow as possible.

An example of these effects is shown in Figure 2. Eclipse entry begins at 0934:30 UT. Transient effects of this entry are over by 0938. The X and Y offsets between these two times are approximately 12 and 18 gamma, respectively. Since no solar cell currents are flowing at this later time, we assume the measured

field is exactly equal to the natural field. Thus, the correction vector (C_X, C_Y, C_Z) to be added to the data for the particular state of the spacecraft on entry to this eclipse has X and Y components of 12 and 18 gamma.

The effects of losing the signal from the sun sensor and cooling of the spacecraft are also apparent in this figure. Large amplitude sinusoids in X and Y gradually increase in frequency as the assumed spin frequency departs from the actual frequency. At about 1045 the satellite emerges from eclipse and the measured field is again comparable to the field before eclipse.

Determination of Parallel Offsets in the Eclipse State. In contrast to the situation for the transverse sensor, there is no equally satisfactory method of determining the offset in the parallel sensor. The method we use is based upon the assumption that the natural field will be the same at a fixed point in the magnetosphere provided the solar wind parameters remain fixed. The local time for which the effects of changes in these parameters will be the least in the synchronous orbit is at local noon. Thus, we take the average of the field measurements in the parallel sensor at local noon on quiet days for a given state of the spacecraft. On the basis of previous reports, Sugiura et al. (1970), Fairfield (1968) and Russell (1970), we take the field at this point to be about 120 gamma. The difference between this value and our observations is the correction to be applied to the parallel component for this spacecraft state.

Absolute Correction for Three Equinoxes. The results of

our determination of absolute corrections for three successive equinoxes after launch are shown in Table 2. This correction vector differs from the example above because of a difference in spacecraft state. The standard deviations shown for each component of the correction vector represent the variation in the offset for about 10 separate measurements. The large absolute variation in the Z component of the correction vector is due to the effects of differing solar wind parameters on supposedly similar quiet days. It should be noted that the percent error in all three corrections are comparable. Also, we note that the ambient field at ATS 1 typically has perpendicular and parallel components of 25 and 100 gamma. Consequently, the percent errors in the corrected field components are not significantly different.

It is also important to note that the three successive determinations of offsets are the same within the indicated experimental error. As a consequence, we have considerable confidence in the values obtained.

Spacecraft States and Associated Correction Vectors

Determination of Spacecraft State. As mentioned previously, the state of the spacecraft changes frequently as commands are sent turning the various subsystems on and off. The currents flowing either in the circuits of the spinning spacecraft or in the inertially fixed solar cells change due to different power requirements. Thus, for each new state of the spacecraft a new correction vector is required.

An example of the effects of these changes is shown in the right panel of Fig. 3. The rate at which these changes occur as well as the

magnitude of their effects creates a serious problem. In our initial attempts to find consistent correction vectors for various states, we discovered that almost all of the communications subsystems as well as the cloud camera affect the spacecraft field. In addition, we have found that in some cases the order, i.e., time history, of the commands is important.

As a result of these observations, we found it necessary to create a complete time history of the spacecraft state. Since a complete log of all commands sent to the spacecraft is kept by the ATS operations office of Goddard Space Flight Center, it was possible to create such a history. Our initial attempts to do this failed, however. We found that our final keypunched version of the command log had innumerable errors. These errors were consequences of human mistakes in every step of the process of producing the log. The first two steps were relatively simple. We checked for valid command numbers and time sequence. After this step we developed a spacecraft state simulation program.

The purpose of this program was to detect inconsistencies in the sequence of commands. For example, a command to change the mode of a subsystem which was supposedly off is inconsistent.

In order to remove inconsistencies such as the one in the preceding example, we found it necessary to scan both the later log and the uncorrected magnetometer data. When a number of other commands manipulating the same subsystem were found, it was assumed that a command was missing from the log. If the command was one which was known to affect the magnetometer, the uncorrected data were scanned to locate the time the command must have been sent.

In many cases, commands were added or deleted in order to produce a consistent command log. In a number of cases the decision of how to remove the inconsistency or where to place the pseudo-command was arbitrary.

The above procedure, while creating a consistent log, cannot guarantee a completely accurate one. Fortunately, most of these problems involve subsystems whose states were changed a number of times per day so that any errors in the state do not persist. In addition, such errors, if they affect the magnetometer, become evident in the final, corrected data and appropriate corrections can be made to the spacecraft state.

Several pages from our current listing of the spacecraft state log are shown in Table 3. Note these pages include the time interval of the eclipse of Figure 2. In the box at the top left of the page is a textual description of the

spacecraft state at the time of the first command listed. At the top right of the box is an interpretation of the listing. Successive times down the page are times the commands in the second column were sent. The third column interprets the command number. The next four columns give a textual description of the state of the major subsystems. The next column, containing three groups of eight characters, is a hexadecimal listing of the spacecraft state vector. When this vector is expanded into a binary number, the successive bits represent on-off states of the various subsystems as well as the order in which some of these were turned on. The next column is a flag presently not used. The final three columns are the three components of the correction vector which must be added to the measured field to obtain the actual field for the state. The flag 3333.3 indicates the correction is not presently known.

Additional information about this listing is contained in Tables 4 and 5. In Table 4 all possible commands sent to the spacecraft are listed in increasing order (note their octal base). In Table 5 we give a complete description of the spacecraft state vector and its interpretation.

As a measure of the magnitude of the task discussed above, it should be noted that during the first two years of operations there were 60,000 commands sent to the spacecraft.

Determination of Relative Offsets. Once the state vector was known it became possible to determine the changes in the field as transitions between states occurred. Conceptually,

the procedure is simple. Referring to Figure 3, all that is necessary is to measure the changes in each component of the field during the transition. In practice, the large number of states and errors in the measurements make this an almost impossible task without computer assistance.

The automated procedure which we developed is the following. Using a data set (in this case disk storage) containing the state vector, we read through the uncorrected magnetic field data tapes. At each point where a transition occurred the data were read into core memory. Since the accuracy of the command log is only ± 5 seconds and the magnetometer time resolution is 0.16 seconds, it was necessary to locate the exact time of the offset. If this time was located, averages of the measured field vector before and after the offset were made and subtracted. This change in the correction vector was recorded on an output data set along with the state vector before and after the offset. If no clear indication of the offset was found, the event was discarded. Similarly, if two transitions occurred less than 5 seconds apart, the event was also discarded.

The preceding data set was then sorted, first according to initial state and then according to final state, and finally by the magnitude of the offset in the Z component. This data set was then scanned using the UCLA interactive console system. Events for which the magnitude of the offset in any of the three components was radically different from the typical values for the group were deleted manually. The edited data set was then processed by computer, creating averages and standard deviations for each

group containing the same initial and final states. The standard deviation for each group was then used to reject any values more than 1 standard deviation away from the mean for the group. Finally, averages and standard deviations were determined for each group in the final version of the data set.

The justification for the above procedure is based on the observation that many of the calculated offsets were clearly in error. These errors were due to difficulties in locating the exact time of offset, transient fields during the change in state, and natural fluctuations in the field.

Determination of Most Frequent States. An examination of the data set of average offset vectors between vector states revealed that there were many state transitions that did not change the spacecraft field. On the basis of these, we were able to determine which subsystems were unimportant. This, in turn, allowed us to "mask" certain bits in the spacecraft state vector as unimportant (refer to Table 3 for explanation of vector).

The next step in the procedure was to read through the state vector tape, determining the total length of time the spacecraft existed in each state. In this process we used the "equivalenced" state vectors, i.e., state vectors in which the unimportant subsystems were masked in the sorting procedure. A listing of these states is given in Table 6. These states are listed according to decreasing total time the spacecraft was in the indicated state. The final column of this table indicates the percent of the total data that can be corrected if all the correction vectors to this point in the table are known.

It is evident from examination of Table 6 that 95% of the data can be corrected with only 45 of the state vectors known. Clearly, there is a point of diminishing return in which the labor involved in determining the correction is more lengthy than the amount of data gained. The heavy line across the table represents our arbitrary cutoff point.

Determination of Absolute Correction Vectors for Most Frequent States. Using Table 6, we have been systematically determining the correction vectors for states of decreasing total duration. Our method is a manual one and proceeds as follows. We begin with the correction vector for the eclipse mode determined as discussed previously. We then use the listing of state transitions and associated changes in the correction vector to determine the correction vector for nearly identical states. Proceeding in this way, we establish a tree of related states and their absolute correction vectors.

Clearly, as states become progressively more distant from the eclipse state, the errors in the absolute correction vector become larger. However, the fact that single commands turn off a number of subsystems simultaneously guarantees that no state is too distant.

Automatic Correction of Magnetometer Data

Correction Procedure. The data set containing the state vector and associated correction vectors is sufficient information to correct the data at 15 second time resolution. A data tape containing uncorrected magnetic field data at 0.16 time resolution is read into the computer memrory. Fifteen second averages of each measured field component are created. A comparison of the time of this average to the state vector listing determines the appropriate correction vector to be added to the calculated averages. The particular average including the time of transition between states is flagged.

The corrected fields are obtained in spacecraft coordinates in which the Z axis is parallel to the satellite spin axis, the sun vector lies in the XZ plane, and the Y axis completes the right-handed system. Note the spacecraft is located in the earth's equatorial plane with its spin axis as close to parallel to the earth's rotation axis as possible. Consequently, the XYZ coordinate system of spacecraft coordinates is equivalent to geocentric solar earth equatorial coordinates (Russell, 1971). In the XYZ system the coordinate axes rotate once every 24 hours with respect to a magnetic meridian plane. Consequently, the data are transformed to the rotational VDH coordinate system. In this system H is still parallel to the satellite spin axis as was the Z axis of the XYZ system. The V axis is radially outward and D is azimuthally eastward in the equatorial plane. In this rotational VDH system the dipole field at ATS 1 has

constant components of (-7, 22, 107). These constant offsets are somewhat inconvenient so another transformation is made to produce the dipole VDH system (Russell, 1971). In this system H is antiparallel to the earth's magnetic dipole axis and V radially outward in the magnetic equatorial plane. Since the location of ATS 1 at 150° W longitude is almost exactly at the intersection of the rotational and magnetic equatorial planes this transformation is nearly an 11° rotation about the V axis. In addition to the above, another transformation is made when the spacecraft spin axis is not parallel to the earth's rotation axis. This transformation is applied immediately after corrected field values are obtained in spacecraft coordinates and converts the field to GSEE coordinates. The format of the final corrected data tapes is shown in Table 7.

An example of data corrected by the above procedures is shown in Figure 3. The right-hand panel shows the uncorrected data and the left-hand panel the corrected field in dipole VDH coordinates. The V component is approximately -7 gamma, the D component nearly 0, and the H component about 115 gamma. The missing data after 0330 are due to unknown correction vectors associated with several transition states of short duration. The pulses apparent in all three components are due to the spin scan cloud camera. As discussed in the next section, we are presently unable to correct these pulses. We also note that the correction at 0344 is not quite right.

Another example of automatically corrected data is shown in Figure 4. Here 2-1/2 minute averages for the entire day have been plotted. Spikes in all three components are the effects of the spin scan cloud camera pulses shown in Figure 3 at higher time resolution. Infrequent small offsets in the three components are consequences of turning the camera on or off. Finally, the large offsets in the H component are due to incorrect correction vectors associated with the VHF transmitters. Despite the remaining difficulties the data plotted in Figure 4 represent a considerable achievement. To obtain similar but less accurate results by our previous hand corrections would involve more than a week of labor. The following section discusses the remaining problems to be solved.

Remaining Problems

Several problems in the automatic correction of data remained to be solved. The most serious of these is the effects due to the spin cloud camera. The camera takes approximately 22 minutes to complete a scan. Then during 2-1/2 minutes it resets for another scan. Fairly large offsets are associated with the reset mode. Somewhat smaller offsets are associated with turning the camera on and off. The magnetic effects of the reset mode have been found to be functions of universal time. This apparently results from the fact that the camera operation is synchronized in such a way as to obtain the picture of the earth at any local time. In other words, the magnetic effects are organized in the rotational VUH system rather than the XYZ system based on the sun vector. However, our correction procedures must be carried out on data in the XYZ system.

Another problem is that the actual time between scans is not constant interval but a constant number of spacecraft rotations. Consequently, the repetition period varies with the spin rate.

Still another problem is the fact that the camera starts or stops wherever it is in its cycle when an on or off command is received. This makes it particularly difficult to predict when the first reset mode will occur.

The VHF transmitters on the spacecraft also cause considerable difficulty. As power to these is turned on, large offsets occur which decay asymptotically in about 15 minutes

to a smaller offset. In addition, transitions between states appear to be considerably more variable when the VHF transmitters are on.

IV. CALCULATION OF POWER SPECTRA USING DATA WITH VARIOUS TYPES OF INTERFERENCE

Types of Interference. As discussed in the introduction, there are a number of forms of spacecraft interference which appear in the output of the magnetometer. These include the DC offsets discussed in the previous section, data gaps, noise spikes and periodic signals. Each of them introduces difficulties when an attempt is made to calculate power spectra. We have found, however, that a relatively simple procedure enables us to derive most of the spectral information without the necessity of initial corrections. The nature of these difficulties and our procedures are discussed below.

Figure 5 displays magnetometer data at the highest meaningful time resolution 0.32 seconds. In this figure the vertical scale is 5 gammas per division and the horizontal scale is 5.12 seconds per division. This choice of horizontal scale is determined by the satellite telemetry rate which completes one sequence per 5.12 seconds. In each sequence there are sixteen 0.32-second averages. At the bottom of the figure, textual material presents time and 1.28 second averages of each component of the measured field. The coordinate system is essentially geocentric solar earth equatorial coordinates as described in the previous section.

One type of interference occurs at 0335:00.8 where there is a DC offset in all three components of the field. This offset

should be compared to the same offset plotted at 15 second time resolution in Figure 3. Spectral analysis of raw data containing such offsets results in spectra which show little besides the Fourier resolution of a sequence of random step functions.

Another type of interference appears at 0335:31.5 where a gap in the data is flagged by a large number. Spectral analysis of the raw data would simply give the Fourier resolution of a large pulse. A similar, though less important problem occurs at 0333:51.6 where a small noise spike in the Y component appears.

Still another problem is a high frequency interference signal of several gamma amplitude present throughout the data. The signal is most obvious in the Y component as a ramp function of 5.12 seconds duration. The ramp is clearly correlated with the boundaries between telemetry sequences. Since a ramp function has a Fourier spectrum containing all harmonics of the repetition period, the power spectrum of these data contains a sequence of harmonic spectral lines with the fundamental at (1/5.12 Hz).

A similar interference signal at lower frequency occurs only in the parallel (Z) component. At 0335:16.2 a two gamma jump in Z is the beginning of a 16 sequence (81.2 sec) ramp. Spectral analysis of decimated data, i.e., 10 second averages, also produces harmonically related spectral lines due to this ramp.

As discussed in the introduction, the source of these interference signals is the spacecraft. The problem is compounded by the lack of a boom for the magnetometer. The origin of the offsets parallel and transverse to the spin axis was discussed in the

previous section. The origin of noise spikes and data gaps is usually transient fields which the basic magnetometer responds to but which are mostly filtered out of the final signal by sampling filters. As discussed in a report by Barry and Snare (1966) the high sensitivity and wide dynamic range of the magnetometer is achieved through a coil system which adds constant increments of field to the sensor to keep it in center range. If a transient field forces the magnetometer to change levels, i.e., add field for more than the time between successive readouts of the level, then a gap is introduced in the data with the basic data processing program. This is necessary because levels are read out only one-fourth as often as the basic magnetometer. When two successive readouts of the level are different, it is not known where in the intervening four data points the level change occurred. If the transient causes the level to change twice between readouts returning to its original value, only the sampling filters recognize this change and a noise spike results.

The exact origin of the periodic interference signals has not been investigated. They are almost certainly the result of other environmental measurement experiments whose operations are synchronized by the satellite telemetry rate. For example, particle detectors scan energy with a repetition period which is a fixed number of telemetry sequences.

Techniques of Spectral Analysis

The problems discussed in the previous section make it impossible to perform spectral analysis on the raw data. As a consequence, we have developed several strategies which allow us to avoid these problems. The most straightforward of these is to hand correct the data. This process is laborious and as a consequence limited to decimated data, for example, 15 second averages, where there are fewer points needing correction. This process is carried out by making a printer plot similar to that shown in Figure 5 for the decimated data. Times of bad points are then identified, gaps interpolated, and offsets measured. This information is keypunched and fed to a control program which carries out the appropriate operations at the times determined by the scanning process. The time series resulting from this is free of errors so spectral analysis is carried out in the normal way.

The second procedure is more subtle and justified by mathematical theory developed by Parzen (1962). Intuitively, it seems that it should be possible to use the available data in time series containing gaps to determine a spectrum. The standard technique of spectral analysis discussed by Blackman and Tukey (1958) begins with the determination of the correlation functions. For example,

$$C_{XX}(k) = \frac{1}{N-k} \sum_{j=1}^{N-k} X_j \cdot X_{j+k}$$

Here X_j represents the Jth sample of some variable in the time series X. For a given lag k the correlation function is a single number determined by a sum of cross products over the

entire time series. If a few points are missing in the time series, it will not change the correlation function by much if the normalization constant 1/(N-k) is adjusted to be the total number of available cross products.

If the correlation function is calculated in the preceding manner we can Fourier transform it without further problems and obtain the power spectrum. It can be shown that this procedure is entirely equivalent to that described in the paper by Parzen (1962) and is mathematically justified.

It should be recognized that although this process handles gaps, spikes and offsets remain serious problems. To deal with these we have introduced an additional step in the determination of spectra. We begin by calculating the first difference time series, subtracting the jth point from the j+1th point and dividing by the time separation. This process approximates the derivative operation at low frequencies. The first difference time series has zero mean, offsets appear as spikes, and spikes appear as a pair of oppositely directed spikes. Gaps widen and the flags are set to 0 (the mean of the first difference time series). In the next step we pass through the series setting all spikes larger than a specified value to 0. This new series has no remaining problems except gaps and may then be analyzed by the technique described above. The resulting spectrum must be corrected, however, for the effects of the first difference operation. This is done by dividing each power spectral estimate by the reciprocal of the square of the transfer function of the first

difference operator. This process is called recoloring and produces the spectrum of the original undifferenced data.

It should be pointed out that in addition to eliminating the problems of spikes and offsets there are other advantages as well. For example, geophysical spectra typically have steep power law decreases in power with increasing frequency. The usual Blackman-Tukey technique of spectral analysis is particularly sensitive to distortion of higher frequency estimates by power at low frequencies. The first difference operation effectively decreases the slope of the spectrum. For example, a $1/f^2$ spectrum of the original data becomes a flat spectrum.

There is one remaining limitation on the above procedure. The Blackman-Tukey technique is exceedingly slow and expensive to use on a computer. An alternative procedure uses the fast Fourier transform (FFT) algorithm developed recently by Codey and Tukey (1965). In this procedure the first difference time series is Fourier transformed by the FFT algorithm and spectra determined directly from the Fourier coefficients. The disadvantage of this process is that data gaps appear as modulation of the original time series. This modulation may be thought of as multiplication of the original time series by a function whose value is either 1 or 0 depending upon whether data are available or not. By a fundamental theorem in Fourier analysis, multiplication in the time domain becomes convolution in the frequency domain. In other words, the power spectra obtained using the FFT are distorted by the convolution of the spectrum of the modulation with the spectrum of the undistorted time series.

Empirically we find that for most of our work to date this distortion is not significant. This fact can be shown by comparing the spectra obtained using the FFT and the modified Blackman-Tukey technique described above. It can be understood theoretically by recognizing that the Fourier spectrum of a modulation function consisting of a sequence of 1's interspersed with a short sequence of 0's randomly spaced is sharply peaked at zero frequency. Convolution of this spectrum with any arbitrary spectrum does not produce significant changes.

Example Spectra. An example of cross spectral analysis of first difference time series with the FFT technique just described is shown in Figure 6. The original data are taken from a quiet day and are essentially the same as that shown in Figure 5. In calculating these spectra we have used data at highest meaningful time resolution, 0.32 seconds, to emphasize the high frequency portion of the spectrum. Also, the spectra in this figure have not been recolored.

Examining the top left panel, we note a peak in the spectrum at 0.4 Hz. This peak is a consequence of two factors. The steep fall off above this frequency results from numerical filters applied in the basic demodulation program to reject the approximately 1.6 Hz spin frequency of the satellite. The slower fall off at low frequencies is the result of the first difference operator discussed above.

In the top right panel the same spectra are plotted with a linear frequency scale. At approximately 0.2 Hz a very sharp spectral line appears at the frequency corresponding to the

satellite telemetry sequence. Also apparent are a number of harmonics of this line at higher frequency.

The bottom right panel shows the coherency between the indicated pairs of components. The harmonic lines are particularly apparent in this display.

Another example of spectra is shown in Figure 7. The original data include large amplitude, irregular pulsations at ATS 1. These spectra differ from the previous example in that they have been recolored for the first difference operator. Also, eigenanalysis has been carried out on the spectral matrix obtaining principal axis coordinates at each frequency. In the top left panel the dashed line labeled "quiet" is the trace of the spectral matrix on a quiet day. Note the steep decrease above 0.4 Hz is still apparent.

At the top right it is quite apparent that the spectra lines are distinct from the remainder of the spectrum. Their narrow width and high polarization (bottom right panel) distinguishes them from typical geophysical phenomena. A final example of spectra is shown in Figure 8. In this case the original first difference time series was decimated creating six second averages in order to study lower frequency waves. The sharp spectra line at 0.01 Hz is a natural signal of unusually narrow bandwidth. On the flank of this peak at 0.0122 Hz is the fundamental of a 16 telemetry sequence ramp in the Z component of the original data.

V. SCIENTIFIC RESULTS

1. Storm Time Meridional Oscillations

Quasi-sinusoidal magnetic field oscillations (micropulsations) are regularly observed at ATS-1 during geomagnetic storms. The wave events typically occur during the main phase and tend to be confined to the afternoon sector. Detailed analysis of 3 such storm time events was discussed by Barfield et al. (1971). Preliminary results of a statistical survey of all the storm time events observed during 1967 have corroborated the earlier conclusions of Barfield et al., and are presented here.

The statistical survey included some 21 events which were well enough defined to be recognizable from a visual scan of the magnetometer data. An "event" was defined as any period of time in which at least 5 cycles of a wave were present. During some events, the oscillations actually subsided for a time equivalent to several cycles, but in each case they began again with no significant change in the oscillation characteristics.

The occurrence statistics of the observed events show that the oscillations occur most often during the main phase, usually near the main phase minimum. In addition the local time distribution of the events is such that the oscillations have a maximum probability of occurring just prior to local dusk with a sharp cutoff at dusk.

The observed events typically began abruptly, lasted approximately one hour and ended suddenly. A close correlation with substorm expansions was observed for the bulk of the observations and in addition, the majority of the event onsets were briefly preceded

by a rapid decline of the field strength at the satellite. Those events which did not exhibit substorm correlation typically followed an enhancement of the main phase decrease at the satellite.

Spectral analysis of the observed events indicate that the frequency of the waves may range from .003-.007 Hz, and the most probable frequency is ~.005 Hz. The waves tend to be linearly polarized with the axis of polarization lying in a plane roughly defined by the magnetic meridian plane.

The preliminary results of the study suggest that the observed stormtime oscillations may be generated by an instability of the enhanced stormtime ring current, and the associated hot ($\beta \gtrsim 1$) plasma. It has been observed that the ring current is strongest during the main phase of the geomagnetic storm reaching a maximum intensity at the main phase minimum (Frank, 1967). Further, it is thought that the partial ring current attains its maximum strength during the main phase, with a longitudinal extent from midnight westward to the afternoon sector. The fact that the observed waves occur only during storms, primarily during the main phase, and in the afternoon sector lends strong support to the possibility that they are associated with a ring current instability.

Recent work by Crooker and Siscoe (1971) using magnetometer data from a chain of low latitude ground stations, has shown evidence that during disturbed times the maximum depression due to the partial ring current is near 1800 LT. They conclude that the position of this maximum depression, presumably indicative of the azimuthal location of the maximum of the partial ring current, may vary as much at 45° from 1800 LT. The local time probability distribution

derived from the work of Crooker and Siscoe agrees well with the local time occurrence distribution of our observations, that is the percentage of events observed at a given local time (in the afternoon sector) corresponds roughly to the probability that the maximum ring current effect is at that local time. This is true for the afternoon sector only; the results of Crooker and Siscoe shown the distribution of the maximum ring current nearly symmetric about 1800 LT, while the observed ATS-1 events have a sharp cut-off at dusk.

The source of the assymetry of our observations about dusk is open to question. However, with the assumption that some other physical mechanism (e.g., change in effective L shell) prevents occurrence of the waves after dusk, the work of Crooker and Siscoe lends strong support to the suggestion that the stormtime oscillations are due to a characteristic instability of the partial ring current.

If the observed wave events are associated with the peak in the partial ring current, as suggested, then the characteristic dip in field strength prior to the events may be viewed as evidence of newly injected plasma brought in by the substorm process. Thus, the responsible instability could be generated by one or both of the concomitant effects of the injection process. First, a fluid instability such as the drift mirror instability (Hasegawa, 1969; Barfield et al., 1971), or alternatively the steep gradients induced by the rapid injection could trigger a gradient associated instability such as the compressional Alfven wave instability (e.g., Cladis, 1971).

The long duration of the wave events coupled with their restricted frequency range and well defined orientation suggests a resonance of the magnetospheric cavity. Whether the duration of an event is temporally or spatially limited is still unclear.

Several suggestions have been made regarding the origin of oscillations similar to those described here, (Sonnerup et al., 1969; Hasegawa, 1969; Lanzerotti et al., 1969; Cladis, 1971). Cladis (1971) suggested that meridional oscillations of the magnetic field could be generated by injection of high energy plasma into the ring current. Such injections would be likely during geomagnetic substorms, as mentioned before (Davis and Parthasarathy, 1967). Sonnerup et al. (1969) suggested that such oscillations could be due to "the particle population sloshing back and forth along the field lines." Hasegawa (1969) suggested the drift mirror instability of the ring current. As pointed out by Barfield et al. (1971), it is not possible to support or deny the plausibility of any of these theoretical proposals solely on the basis of the satellite magnetic field observations.

In summary, the stormtime micropulsations observed at ATS-1 suggest the following model. The spatial gradients of the stormtime ring current are enhanced by newly injected plasma during a magnetospheric substorm. Broad band oscillations produced by an instability of this current are then filtered by the resonant properties of the magnetosphere to produce the observed oscillations. Such a proposed model is attractive and we believe, premature. Several critical question remain to be answered.

Concerning the cause of the instability, all the models proposed predict a well defined correlation between the magnetic field oscillations and the high energy particle population. We have not yet investigated such relationships in detail, although Barfield and Coleman (1970) did note that the energetic protons and electrons fluctuated coherently with the magnetic field for one event of the type discussed here. It is suggested that further investigations are required before a definitive statement can be made concerning the particle behavior during the observed events.

It has also been noted that during many of the oscillation events mentioned, Pc 1 oscillations were observed at ATS-1 (e.g., Barfield and Coleman, 1970). Such high frequency oscillations could be a damping mechanism for the Pc 4-5 oscillations and possible correlations between the two wave classes should be investigated.

The question of the significance of the characteristic dip in field strength prior to the oscillations has yet to be resolved. As previously discussed by Barfield et al. (1971), such a dip would be predicted by the two models considered most likely. If the field decrease does imply a severe field distortion at ATS-1, then the background field geometry prior to and after the dip requires careful study in order to comment on the plausibility of the proposed mechanisms.

Although the observed characteristics of the stormtime oscillations point strongly to the ring current as an energy source for the waves, the point is far from resolved. Two other sources exist at the ATS-1 orbit which would produce a similar field-

particle configuration to that described here. Vasyliunas (1968) has shown that the inner edge of the plasma sheet moves well within the ATS-1 during substorms. Cummings et al. (1969) concluded from a study of quiet time oscillations at ATS-1 that the plasmapause often crosses the ATS-1 orbit. Either of these spatial boundaries could produce the field distortion and steep gradients throught to exist during the stormtime wave events. The importance of each of those possibilities remains to be resolved.

Those events for which no rapid substorm associated field decrease is displayed may be important in that for those cases the enhancement of the main phase decrease might imply entry by the satellite into a region where the distortion exists, rather than a temporal change in the field. The two types of onsets require additional investigation as to the possible implications of temporal versus spatial extent of the resonance, although adequate statistics are not available from the present study.

Another yet unsolved puzzle concerns whether or not the oscillations observed at the satellite are propagated to the ground. For the events studied thus far, auroral zone ground magnetograms were inspected for correlated activity. The results were inconclusive, as in each case there was irregular activity at the ground over a wide frequency range. There were no obvious changes in the ground data correlated with the wave activity at the satellite. Lack of digital data at the ground precluded a comparison of wave spectra.

Intermittent digital ground magnetometer data are now available from the conjugate point of ATS-1, at Tungsten, N.W.T., Canada,

beginning in June, 1969. Spectral comparison of the satellite and conjugate point magnetometer data would be valuable in answering the question of propogation to the ground.

If the observed wave events are in fact standing waves, then a seasonal variation in the orientation of the oscillations would be expected (Barfield and Coleman, 1970). However, for the events studied so far, the bulk of the events were near the equinoxes, preventing any conclusion as to seasonal variations.

In summary, it appears that the stormtime meridional oscillations observed at ATS-1 are a regular feature of the geomagnetic storm, and may provide an effective monitor on the substorm injection process. However, much work remains to be done; a partial list of the necessary tasks is presented in the following section.

2. Ground-Satellite Correlations

For several years the National Science Foundation has supported a magnetic observatory at the conjugate point of ATS-1. This support includes the operation, data processing and analysis of the ground data. Similar support for the satellite data is derived from our NASA grant. During the last year we have carried out preliminary analysis for several distinct wave phenomena observed simultaneously at the ground and the satellite during magnetospheric substorms. The first results were presented by McPherron and Coleman (1971) at the spring meeting of the American Geophysical Union in Washington, D.C. More complete results were presented by McPherron (1971b) at the Fifteenth General Assembly of I.U.G.G. in Moscow. A brief summary of these results is given below.

2A. Transfer Function of the Field Line for Pc 1. A Pc 1 wave event was recorded at the ground station during the expansion phase of a magnetospheric substorm. The local time of this station was near 1800 (dusk). These facts suggest the event was of the IPDP type although a digital dynamic spectrum of the ground signal did not reveal the characteristic upward sweep. Dynamic spectra for simultaneous data recorded at the satellite were also prepared and compared to the ground data. This comparison showed the ground signal was considerably more complex than the satellite signal. This difference was attributed to horizontal propagation of the Pc 1 waves from a number of field lines to the ground station.

Two time intervals when the dynamic spectra showed similar excitation at the ground and satellite were chosen for more careful

study. In one case, the ratio of power at the satellite to the ground was 2.6; in another case, the ratio was 8.6. A possible interpretation of this follows from the fact that Pc 1 waves are presumed to be collimated to a flux tube. If this is true, the signal amplitude must change significantly as a function of position relative to the center of this tube. Thus, a very slight change in the relative conjugacy of ATS-1 and Tungsten could cause a large change at the satellite and almost none at the ground. The implication of this interpretation is that a correct determination of the absolute transfer function will be quite elusive. At best, it seems likely that it can only be determined statistically under the assumption that the largest observed attenuation between satellite and ground occurs when the satellite is centered in the collimated wave.

There exists the possibility of determining the relative transfer function if it can be assumed that the amplitude distribution of various frequency components within the flux tube is the same. Again, this seems unlikely because of the cyclotron instability thought to be responsible for the generation of Pc 1 depends on the equatorial gyrofrequency of the given line, i.e., the lower frequencies are generated at larger L values. Finally, with a single station it is difficult to separate the components of the signal at the ground which are incident above the station and those propagating horizontally.

B. Polarization of Pc 1 in Space. For a number of years the body of theoretical speculation about the origin of Pc 1 has been

based on the assumption that Pc 1 are generated by a cyclotron instability of 1-100 kev protons at about 6 R_e in the equatorial plane. This speculation was justified on a basis of dynamic spectra of the signal obtained at the ground showing the repetition period for pearl-type Pc 1 activity is longer at higher frequencies. This is what is expected for the dispersion relation satisfied by the left-hand elliptically polarized Alfven wave propagating along the field. Ground observations have not been able to establish the validity of this assumption because the ionosphere can reverse the polarization of the Pc 1 signal as it passes through. The observations show both polarizations at the surface. For IPDP events of the same frequency as pearls, it has been generally assumed that a similar source mechanism exists as for pearl pulsations.

We have examined four IPDP events to date and find that all are left-handed elliptically polarized in the equatorial plane at synchronous orbit. Three of these events are positively identified from ground dynamic spectra as IPDP events. While it is recognized that four events are insufficient to decide the question completely, we feel these observations are sufficient to justify the basic assumption of the cyclotron instability of protons gyrating in a left-hand sense, as has been commonly assumed.

C. <u>Pi 2 Noise Bursts on the Ground and in Space</u>. Pi 2 noise bursts are known to be associated with the onset of substorm expansion and have been studied in some detail, but their role in substorm process is not known. From the one event we have examined it appears these bursts may be related to field aligned currents

feeding the westward electrojet.

In an event comprising two bursts recorded shortly before local midnight, we find that sudden decreases in the north-south component of the surface field were closely associated with sudden increases in the east-west component at the satellite. At the ground, a decrease in the north-south field is normally attributed to the westward electrojet while at the satellite the D component variations are usually associated with field aligned currents.

A comparison of power spectra for the ground and satellite data of this event shows comparable spectral density at 0.01 Hz. The surface spectrum falls off rapidly toward higher frequency, roughly as $1/f^3$. In contrast, the satellite spectrum decreases more slowly as $1/f^2$.

A frequently reported feature of Pi 2 bursts is an enhancement of fluctuations at about 0.3 Hz. This enhancement was observed during the two Pi 2 bursts in our event. In both bursts the signals in the horizontal plane were approximately 70% polarized. The polarization was right-hand elliptical with respect to the ambient magnetic field (in the sense of electron gyration). The two bursts differed only slightly in their frequency (0.28 and 0.32 Hz) but had quite different ellipticities (0.2 and 0.5) and orientation (east-west and north-south).

From this very preliminary study we have tentatively concluded that Pi 2 bursts are caused by sudden, perhaps quasi-sinusoidal changes in the field aligned currents driving the westward electrojet. Furthermore, it appears from the distinct polarization characteristics of the 3-second enhancement that this portion of

the burst is of magnetospheric origin rather than an ionospheric cavity resonance as has previously been suggested.

D. Band-Limited Pi 1 Micropulsations. Band limited Pi 1 micropulsations, sometimes called Pi(c), are a regular feature of the recovery phase of substorms in the morning sector. To date, we have examined four events of this type. Two of these were selected from ground data and two from satellite data. For the two events selected from the ground data there was no wave activity at the satellite. In contrast, the two events selected from satellite data did show evidence of corresponding activity at the ground. Unfortunately, for neither of these was digital ground data available. A summary of the results for each of these events is given below.

The first event occurred at ATS-1 on August 17, 1967. The particle data for this event have been examined in some detail by Parks and Winckler (1969). They showed that the fluxes of trapped electrons at ATS-1, as well as precipitated electrons at College, Alaska (650 km west of ATS-1 conjugate point) were periodically modulated at several frequencies. Spectral peaks were seen at frequencies corresponding to periods of 25, 18.3, 9.53, and 6.11 seconds. Dynamic spectral analysis showed that the maximum modulation was 11.3 second period. These observations were made near the dawn meridian during the recovery phase of the magnetospheric substorm.

Using these results as a guide, we have performed spectral analysis over the time interval of the maximum modulation of particle fluxes. We find a pronounced spectral peak at 26

secondswith the rms signal power over the band approximately 0.4 gamma. Doing eigen and coherency analysis on the spectral matrix, we find that the signal was linearly polarized with the major axis orientated 60° from the dipole V axis toward the D axis. The major axis also made an angle of 60° with respect to the H axis. (The dipole VDH coordinate system has H antiparallel to the earth's dipole axis and V radially outward in the magnetic equatorial plane.)

The second event, June 8, 1968, was observed by the OGO-5 satellite as it was inbound across the dawn meridian near the magnetic equatorial plane. The original motivation for studying this event was the fact that OGO-5 passed extremely close to the ATS-1 satellite and magnetic field data were available from it as well. Results of this analysis have been published by McPherron and Coleman (1971) and are only briefly summarized here.

The pulsations were quasi-sinusoidal with period 22 seconds and rms amplitude 0.3 gamma. Their average polarization was transverse to the main magnetic field with the major axis azimuthal in the equatorial plane. The average ellipticity was 0.3 and the predominant sense of rotation right-handed with respect to the main magnetic field (in the sense of electron gyration). Instantaneously, these parameters were quite variable with the pulsations occurring in bursts propagating at various angles with respect to the field. The waves were observed in a region of essentially dipolar field; however, the waves were first observed just inside a sharp transition from a region of continuous field to rapidly increasing field.

No modulation of trapped electrons (E ⩾ than 50 kev) by the pulsations greater than 4% was observed on the same satellite; however, whistler chorus did appear to consist of quasi-periodic burst. Simultaneous magnetic field observations at the ATS-1 conjugate point and also at College, Alaska, showed the pulsations were present on the ground with the same frequency and comparable amplitude. Field observations at ATS-1 did not indicate any wave activity despite the fact that it was clearly present near its conjugate point. It was noted however, that the first OGO-5 observations of these waves were made just inside the ATS-1 orbit. Consequently, it seems quite likely that these waves are radially localized in the equatorial plane and spread somewhat in the ionosphere at the foot of their favored field line. This event also occurred during the recovery phase of a magnetospheric substorm near the dawn meridian.

Two additional events were chosen from digital ground data at the ATS-1 conjugate point, Tungsten, N.W.T., Canada. These events were selected from microfilm plots of micropulsation and bay activity at the ground station. Both events were chosen near the dawn meridian during the recovery phase of substorms. Both events had rms amplitudes of about 1-2 gamma. Also, both events were polarized transverse to the main magnetic field and oriented with the major axis east-west. In contrast to these properties, the two events were quite distinct in their frequency and sense of rotation. One event had a 40 second period and was right elliptically polarized, the other 20 second period and left elliptically polarized. Spectral analysis of the satellite data for both events

showed a completely quiet field.

From the preceding discussion, it is clear that any definite conclusions are premature. However, it seems likely that the waves are spatially limited and that close conjugacy between the ground and the satellite are required before simultaneous observations are possible.

3. Support of Other Projects

A. Field Aligned Currents. During the past year we have continued our study of field aligned currents using the ATS-1 data in conjunction with ground data. Major support for personnel on this aspect of our work is derived from an ONR contract, however, corrected data used in this project are a result of work performed on the NASA grant described herein.

Initial results were presented at the April, 1971 meeting of the American Geophysical Union in Washington, D.C., by Horning et al. (1971). Further work is described in a manuscript under preparation. Briefly, this work studies the simultaneous changes in the H component at ATS-1 and its subsatellite point, Honolulu, during substorm expansions. We find that Honolulu and ATS both observed the same variations in H, an increase near midnight and a decrease during dusk. The simultaneous variations can only be understood in terms of two distinct field aligned current systems flowing on field lines outside ATS-1. The first system, centered in the predawn sector, may be viewed as a collaspe of the near-tail current system by diverting this current through the auroral ionosphere as the westward auroral electrojet. The second system is

centered near dusk and appears to be a similar closure of the partial ring current via field aligned currents through the ionosphere as an eastward auroral electrojet.

B. Multi-Satellite Correlations. Corrected ATS-1 magnetometer data have been used in a multi-faceted study of the substorm sequence. This study shows that the sequence of events thought to occur on a basis of disparate observations of different events by different investigators actually holds for a single substorm event. These results are in agreement with current speculation about the cause of magnetospheric substorms. This speculation suggests that southward interplanetary magnetic fields cause merging of field lines on the dayside of the magnetopause and consequent erosion of flux from the dayside. This flux is transported by the solar wind and added to the geomagnetic tail. The reduced cross section of the dayside increases the angle of attack of the solar wind on the magnetopause boundary. The resulting increase in normal stress reduces the cross section of the near tail despite the fact that it contains greater magnetic flux. As a consequence, there is a large increase in the magnitude of the near tail field. Simultaneously, the plasma sheet near the earth thins and its inner edge approaches the earth.

This sequence of events constitutes what we have called the growth phase of magnetospheric substorms. A detailed presentation of these results is given in a sequence of nine papers submitted for publication in the Journal of Geophysical Research (see nine references under McPherron et al., 1972 , general title: Satellite Studies of Magnetospheric Substorms on August 15, 1968). These

experimental observations in conjunction with numerous other reports in the recent literature form the basis of a quantitative theory of the substorm growth phase worked out recently by Coroniti and Kennel (1971).

References

Barry, J.D., and R.C. Snare, A fluxgate magnetometer for the applications technology satellite, IEEE Trans., Nuc.Sci., NS-13, 1966.

Barfield, J.N., and P.J. Coleman, Jr., Storm related wave phenomena observed at the synchronous, equatorial orbit, J. Geophys. Res., 75 (10), 1943-1946, 1970.

Barfield, J.N., R.L. McPherron, and P.J. Coleman, Jr., A storm associated Pc5 micropulsation event observed at the synchronous equatorial orbit, to be published in J. Geophys. Res., 1971.

Blackman, R.B., and J.W. Tukey, The measurement of power spectra, Dover Pub., 1958.

Buck, H., H.West, Jr., and R.G. D'Arcy, OGO-5 energetic proton observations - spatial boundaries, submitted to J. Geophys. Res., 1971.

Carpenter, D.L., and C.R. Chappell, Correlated OGO-4, OGO-5 and ground observations of some effects of magnetospheric convection, August 13-15, 1968, submitted to J. Geophys. Res., 1971.

Cladis, J.B., Multiply coupled oscillations of field lines in the magnetosphere: modulation of trapped particles and ionospheric currents, J. Geophys. Res., 76 (10), 2345-2356, 1971.

Cooley, J.W., and J.W. Tukey, An algorithm for the machine calculations of complex Fourier series, J. Math. of Computation, 19 (90), 297-301, 1965.

Crooker, N.V., and G.L. Siscoe, A study of the geomagnetic disturbance field asymmetry, Radio Sci., 6 (4), 495-501, 1971.

Coroniti, F.V., and C.F. Kennel, Magnetopause motions, DP-2 and the growth phase of magnetospheric substorms, preprint PPG-99, Plasma Physics Group, UCLA, September, 1971.

Cummings, W.D., R.J. O'Sullivan, and P.J. Coleman, Jr., Standing Alfven waves in the magnetosphere, J. Geophys. Res., 74 (3), 778-793, 1969.

Davis, T.N., and R. Parthasarathy, The relationships between polar magnetic activity DP and growth of the geomagnetic ring current, J. Geophys. Res., 72 (23), 5825-5836, 1967.

Fairfield, D.H., Average magnetic field configurations of the outer magnetosphere, J. Geophys. Res., 73 (23), 7329-7338, 1968.

Frank, L., On the extraterrestrial ring current during geomagnetic storms, J. Geophys. Res., 72 (15), 3753-3767, 1967.

Hasegawa, A., Drift mirror instability in the magnetosphere, Phys. of Fluids, 12 (12), 2642-2650, 1969.

Horning, R.J., R.L. McPherron, and P.J. Coleman, Jr., Correlations between magnetic field changes at ATS-1 and low latitude ground stations, Abstract, SM45, EOS, 52 (4), 324, 1971.

Kivelson, M.G., T.A. Farley and M.P. Aubry, Satellite studies of magnetospheric substorms on August 15, 1968 5. Energetic electrons, spatial boundaries and wave-particle interactions at OGO-5, submitted to J. Geophys. Res., 1971.

Lanzerotti, L.J., A. Hasegawa and C.G. Maclennan, Drift mirror instability in the magnetosphere: Particle and field oscillations and electron heating, J. Geophys. Res., 74 (24), 5565-5578, 1969.

McPherron, R.L., Low frequency waves at ATS-1 and its conjugate point during substorms, Abstract SM44, EOS, 52 (4), 323, 1971.

McPherron, R.L., Substorm wave phenomena, to be published in Proc. XV IUGG Assembly, Moscow, 1971.

McPherron, R.L., and P.J. Coleman, Jr., Satellite observations of band limited micropulsations during a magnetospheric substorm, J. Geophys. Res., 76 (13), 3010-3021, 1971.

McPherron, R.L., Satellite studies of magnetospheric substorms on August 15, 1968, Note 1. State of the magnetosphere, submitted to J. Geophys. Res., 1971.

McPherron, R.L., G.K. Parks, D.S. Colburn, and M.D. Montgomery, Satellite studies of magnetospheric substorms on August 15, 1968, Note 2. Solar wind and outer magnetosphere, submitted to J. Geophys. Res., 1971.

McPherron, R.L., M.P. Aubry, C.T. Russell, and P.J. Coleman, Jr., Satellite studies of magnetospheric substorms on August 15, 1968, Note 4. OGO-5 magnetic field observations, submitted to J. Geophys. Res., 1971.

McPherron, R.L., C.T. Russell and M.P. Aubry, Phenomenological model for substorms, submitted to J. Geophys. Res., 1971.

Parks, G.K., and J.R. Winckler, Simultaneous observations of 5 to 15 second period modulated energetic electron fluxes at the synchronous altitude and the auroral zone, J. Geophys. Res., 74 (16), 4003-4017, 1969.

Parzen, E., On spectral analysis with missing observations and amplitude modulation, Indian J. Statistics, Series A, 383-392, 1962.

Russell, C.T., Geophysical coordinate transformation, Cosmic Electrodynamics, 2 (2), 184-196, 1971.

Russell, C.T., R.K. Burton, and C.R. Chappell, The magnetospheric

field strength and the Alfven velocity as determined by the OGO-5 spacecraft, Abstract SPM101, EOS, 51 (4), 402, 1970.

Scarf, F.L., R.W. Fredricks, C.F. Kennel and F.V. Coroniti, satellite studies of magnetospheric substorms on August 15, 1968: OGO-5 plasma wave observations, submitted to J. Geophys. Res., 1971.

Sonnerup, B.U.O., L.J. Cahill, Jr., and L.R. Davis, Resonant vibration of the magnetosphere observed from Explorer 26, J. Geophys. Res., 74 (9), 2276-2288, 1969.

Sugiura, M., T.L. Skillman, B.G. Ledley, and J.P. Heppner, Magnetic field observations in high β regions of the magnetosphere, Particles and Fields in the Magnetosphere, B.M. McCormac, ed., D. Reidel Publishing Co., 1970.

West, H., Jr., R. Buck, and J. Walton, OGO-5 energetic electron observations-pitch angle distributions in the nighttime magnetosphere, submitted to J. Geophys. Res., 1971.

Vasyliunas, V.M. A survey of low-energy electrons in the evening sector of the magnetosphere with OGO-1 and OGO-3, J. Geophys. Res., 73 (9), 2839-2884, 1968.

Figure Captions

1. Percent data recovered from UCLA magnetometer on ATS-1 since launch in December, 1966. (Refer to Table 1.)

2. Example showing measured magnetic field during eclipse of ATS-1. The Z axis is parallel to the satellite spin axis, the sun vector lies in the X-Z plane and Y completes the orthogonal system.

3. Right panel shows uncorrected magnetic field measurements in X, Y, Z coordinate system, defined for Figure 2. Left panel shows the same data after automatic correction and transformation to the dipole VDH coordinate system. In the VDH system H is anti-parallel to the earth's magnetic dipole axis. V is radially outward in the magnetic equatorial plane and D azimuthal eastwards.

4. Plot of 2-1/2 minute averages of ATS-1 magnetic field produced by automatic correction procedure.

5. High time resolution plot of ATS-1 magnetic field measurements. The amplitude scale is 5γ/division and the time scale 5.12 seconds/division. Successive plotted points are 0.32 second averages. Textual material at the left includes time in the form HHMMSS.S and 1.28 second averages of the measured field components in gamma.

6. Results of cross spectral analysis of 0.32 time resolution magnetic field data. The original time series has been differenced and all gaps and spikes set to zero. Spectral lines are due to a ramp function interference signal containing all harmonics of the 5.12 second telemetry rate.

7. Results of eigen and coherency analysis of spectral

matrix. Spectra have been recolored for the effects of the first difference operator. Note narrow band width and high polarization of spectral lines due to interference signal.

8. Eigen and coherency analysis of unusually narrow band width signal at low frequencies. A sequence of harmonic spectral lines is due to a 16 telemetry sequence ramp function (.0122 Hz).

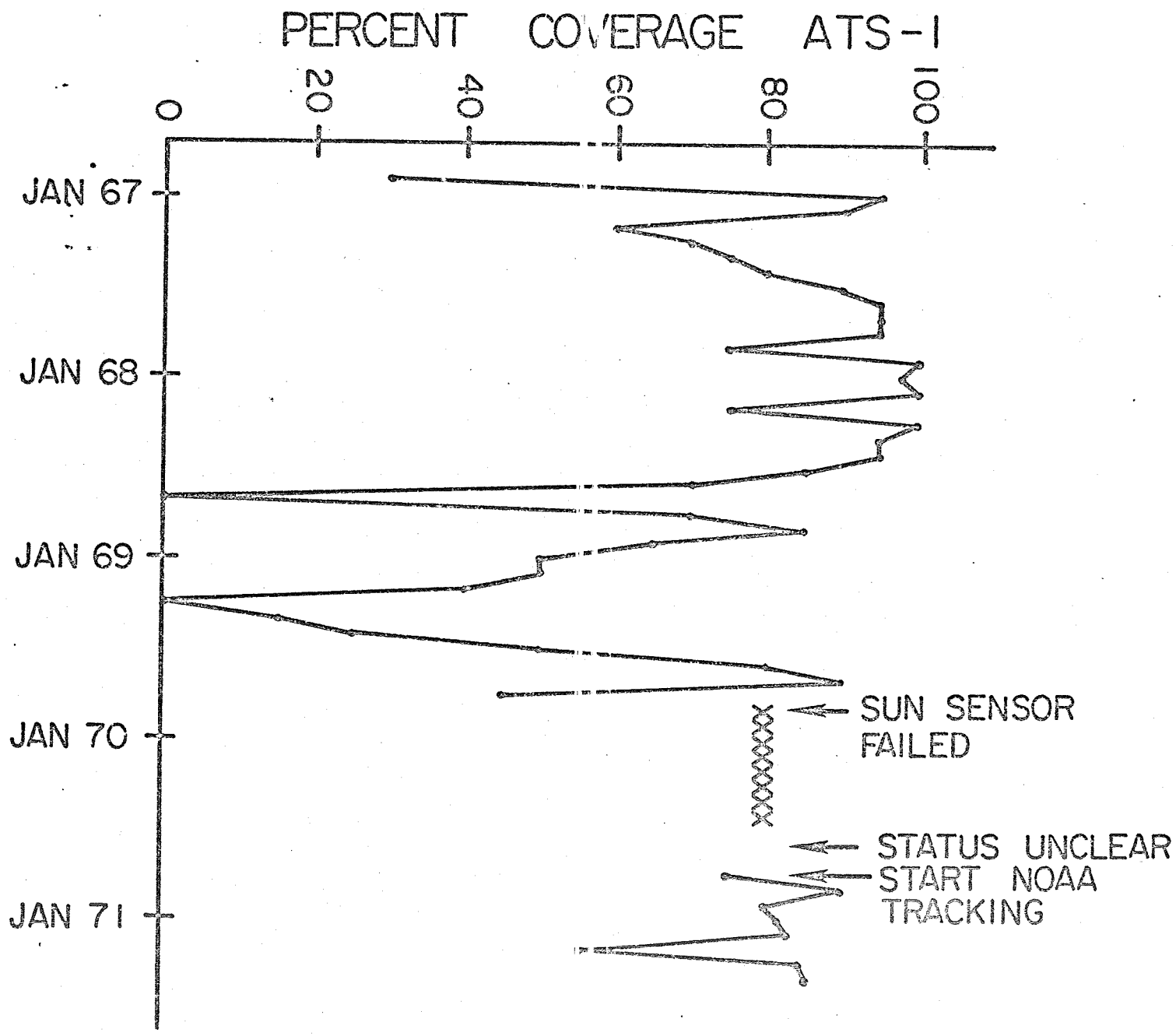
PERCENT COVERAGE ATS-I
0
20
40
60
80
100
JAN 67
JAN 68
JAN 69
JAN 70
JAN 71
SUN SENSOR FAILED
STATUS UNCLEAR
START NOAA TRACKING

Figure 1

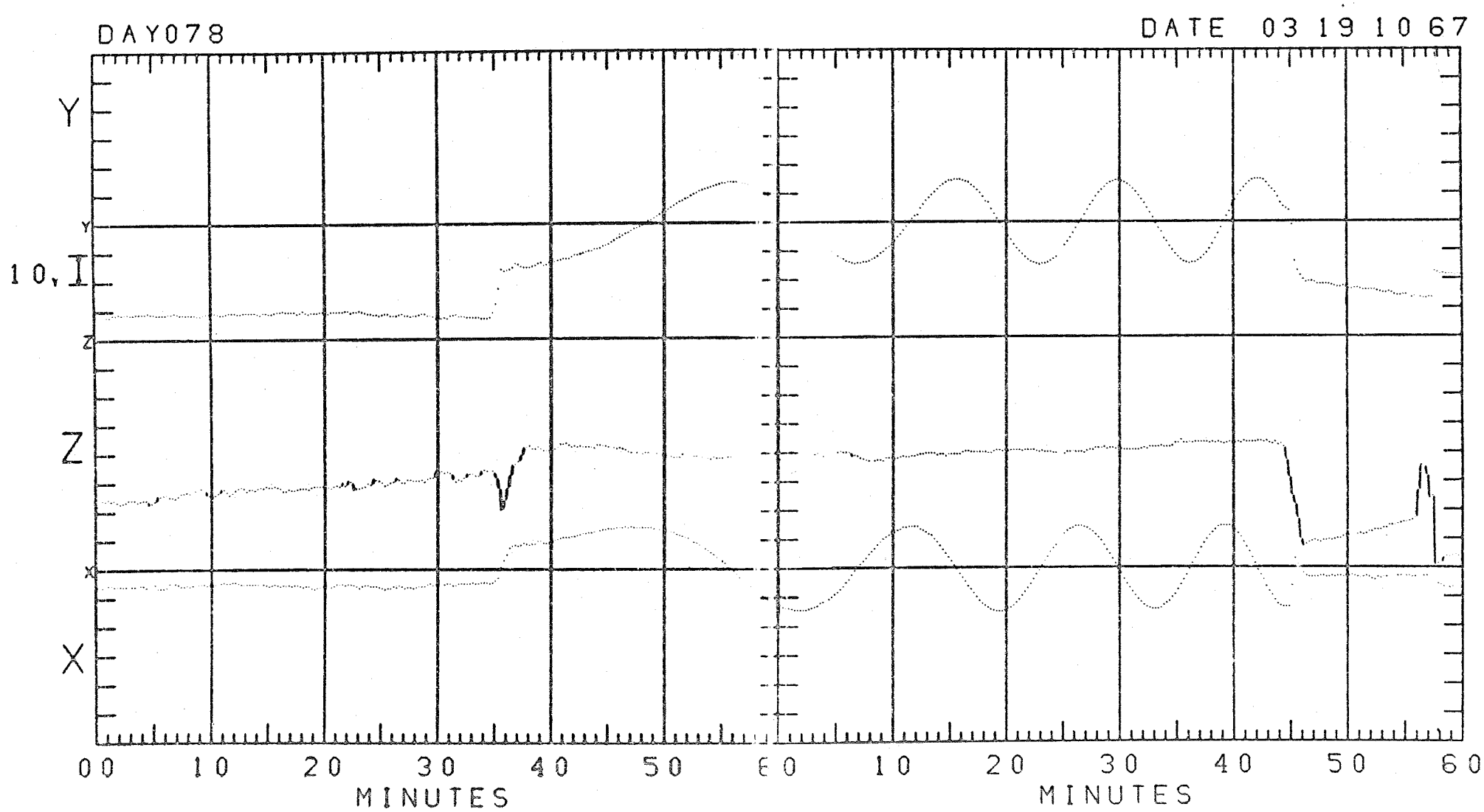
DAY078
DATE 03 19 10 67
Y
10.
Z
X
00
10
20
30
40
50
60
MINUTES
10
20
30
40
50
60
MINUTES

Figure 2

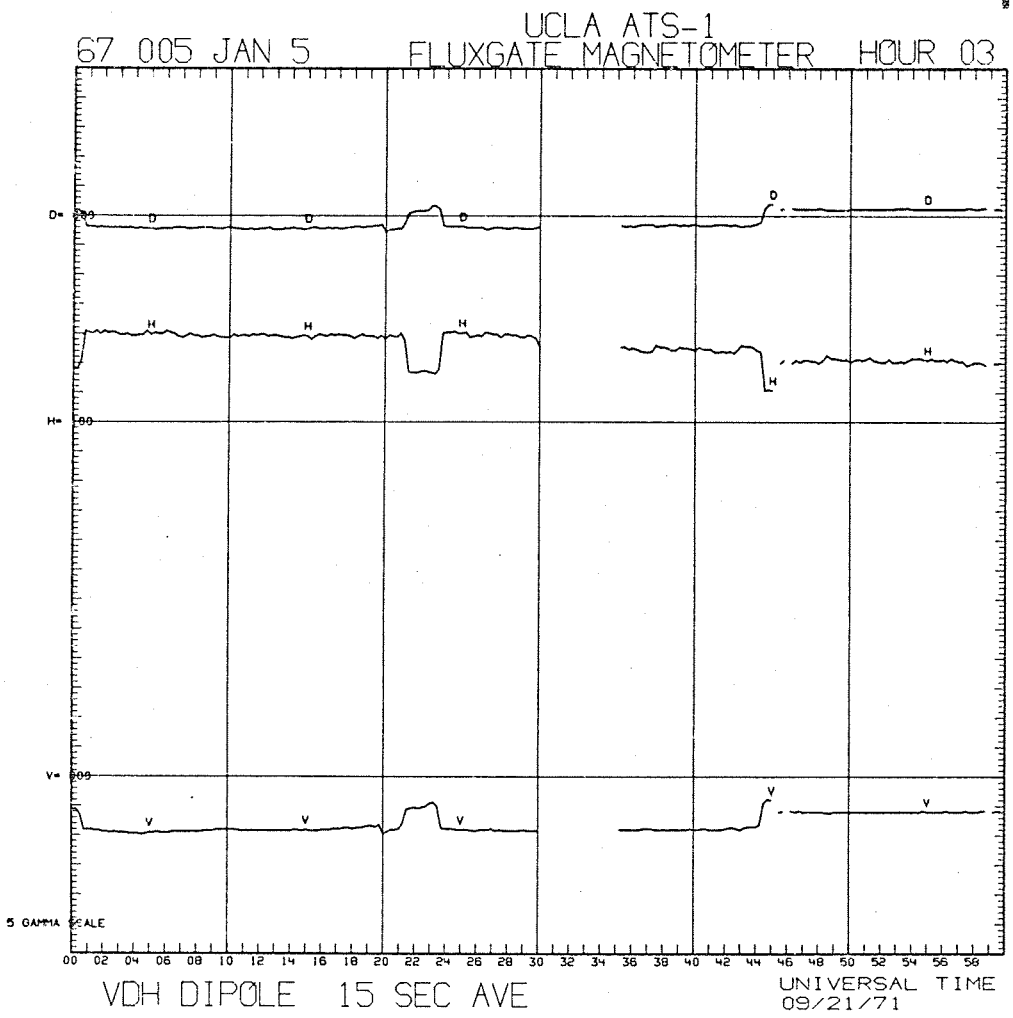
UCLA ATS-1
67 005 JAN 5
FLUXGATE MAGNETOMETER
HOUR 03
D=
H=
V=
5 GAMMA SCALE
00 02 04 06 08 10 12 14 16 18 20 22 24 26 28 30 32 34 36 38 40 42 44 46 48 50 52 54 56 58
VDH DIPOLE 15 SEC AVE
UNIVERSAL TIME
09/21/71

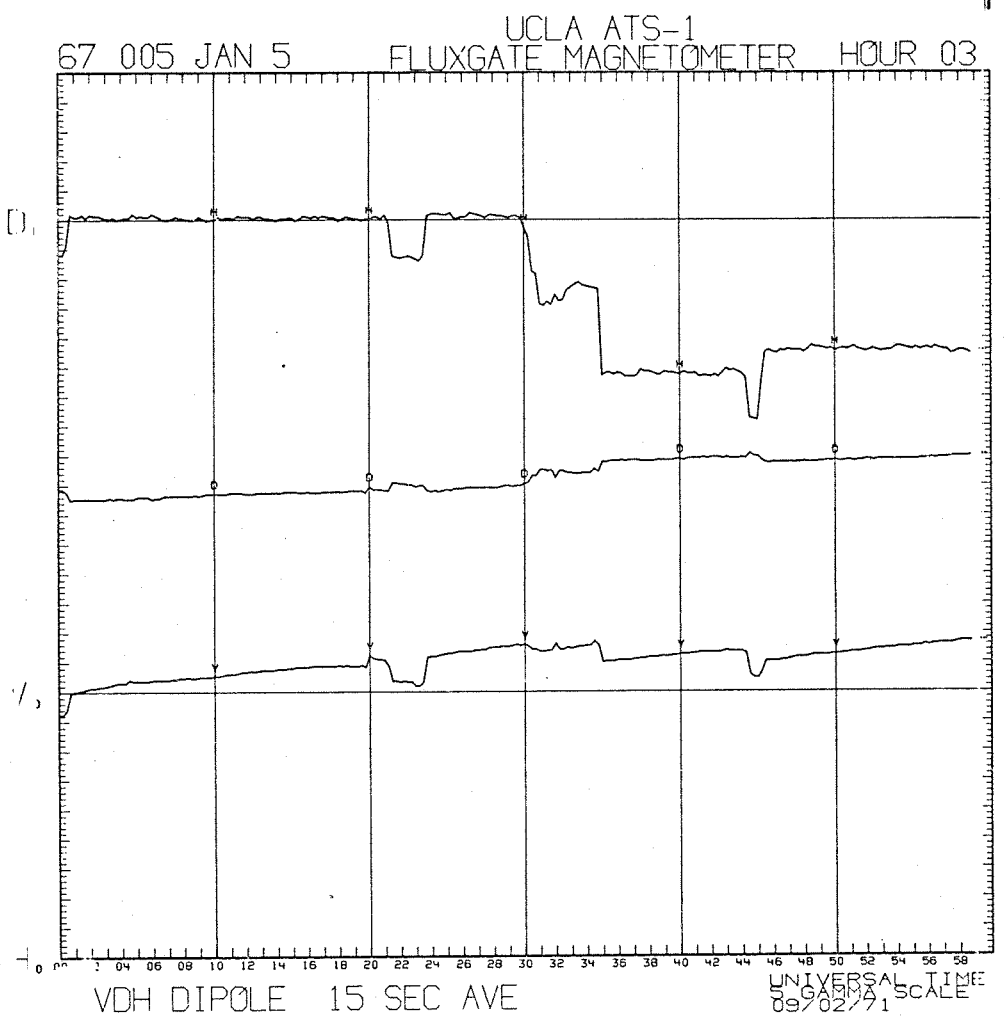
UCLA ATS-1
67 005 JAN 5
FLUXGATE MAGNETOMETER
HOUR 03
04 06 08 10 12 14 16 18 20 22 24 26 28 30 32 34 36 38 40 42 44 46 48 50 52 54 56 58
VDH DIPOLE 15 SEC AVE
UNIVERSAL TIME
5 GAMMA SCALE
09/02/71

Figure 3

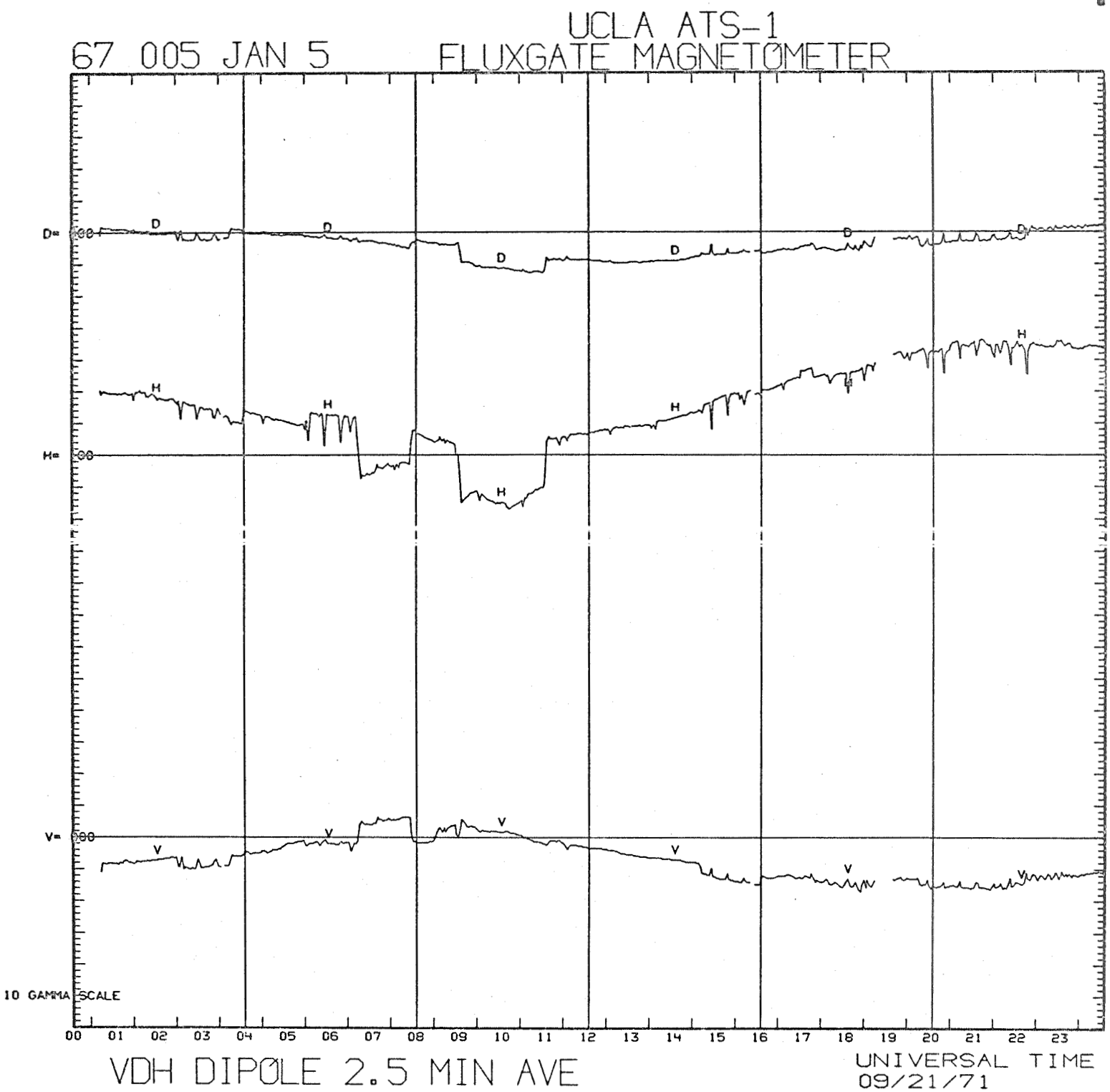
UCLA ATS-1
67 005 JAN 5
FLUXGATE MAGNETOMETER
D=
H=
V=
10 GAMMA SCALE
00 01 02 03 04 05 06 07 08 09 10 11 12 13 14 15 16 17 18 19 20 21 22 23
VDH DIPOLE 2.5 MIN AVE
UNIVERSAL TIME
09/21/71

Figure 4

JAN 05,1967 X OFFSET +20 GAMMAS,Y OFFSET -10 GAMMAS.

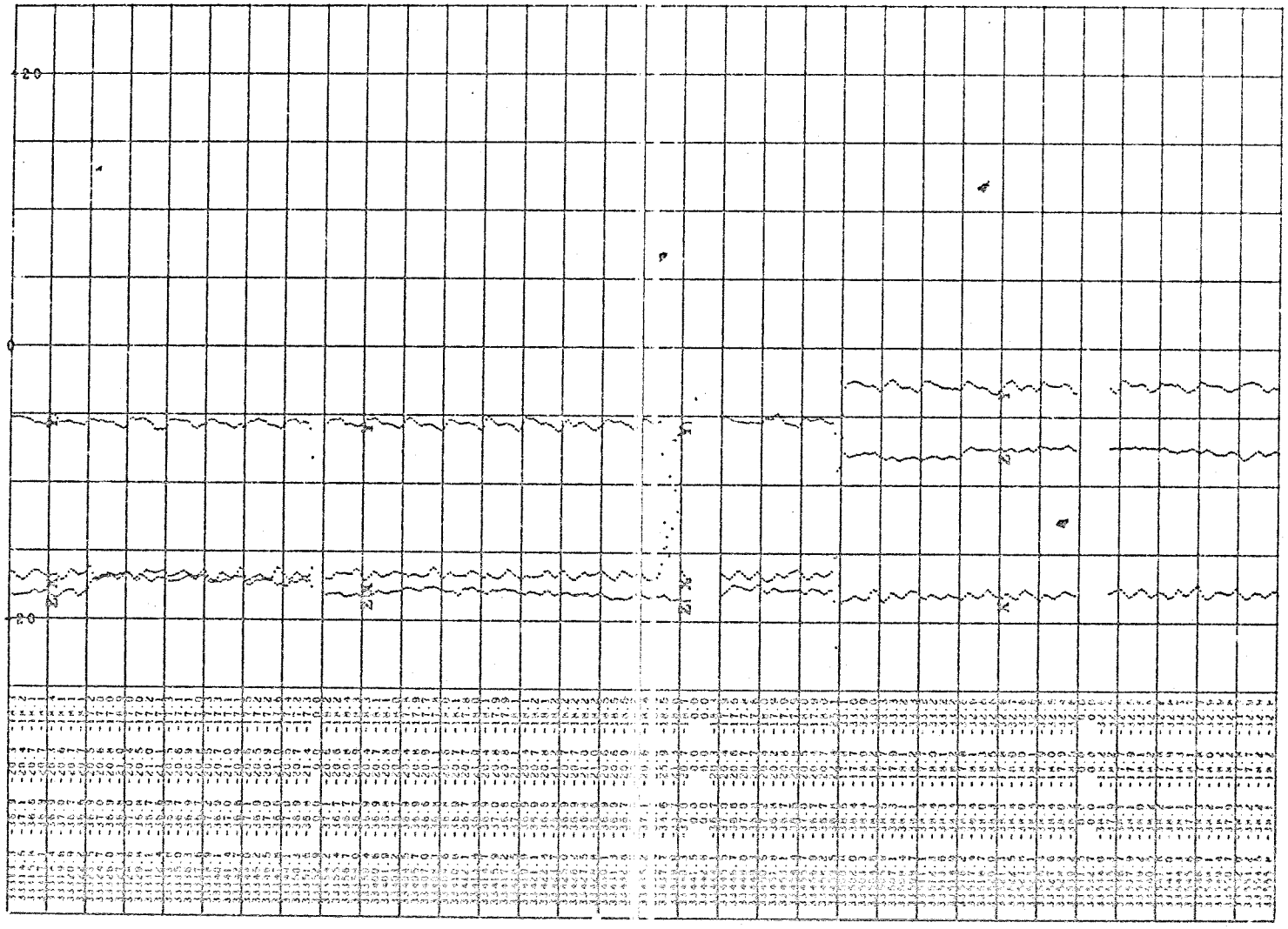

Figure 5

QUIET DATA
0200-0211 UT OCT 9, 1969
UCLA ATS-I MAGNETOMETER

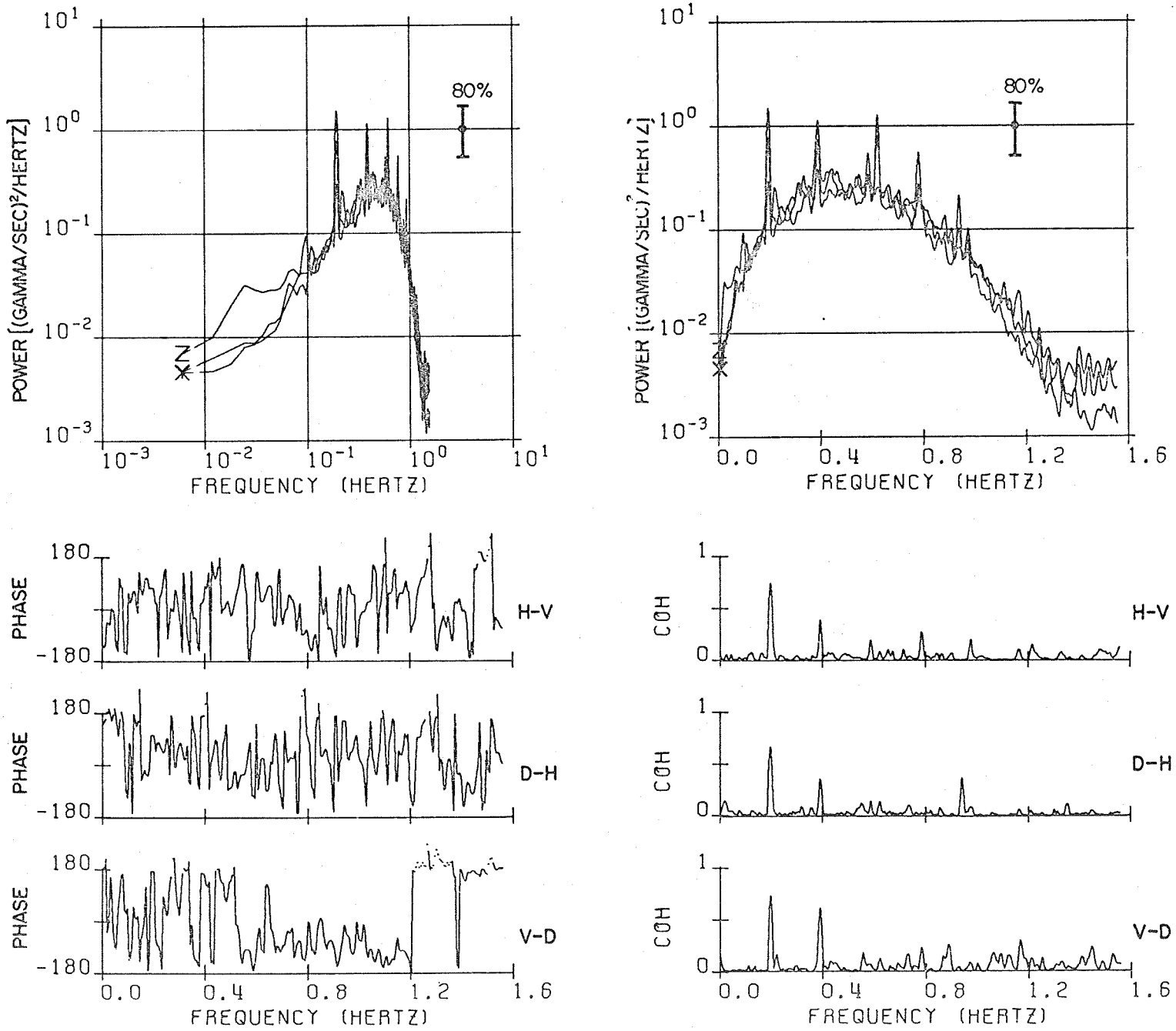

Figure 6

QUIET TIME TRANSVERSE WAVES
1550-2350 UT DEC 18, 1966
UCLA ATS-I MAGNETOMETER
EIGEN AND COHERENCY ANALYSIS

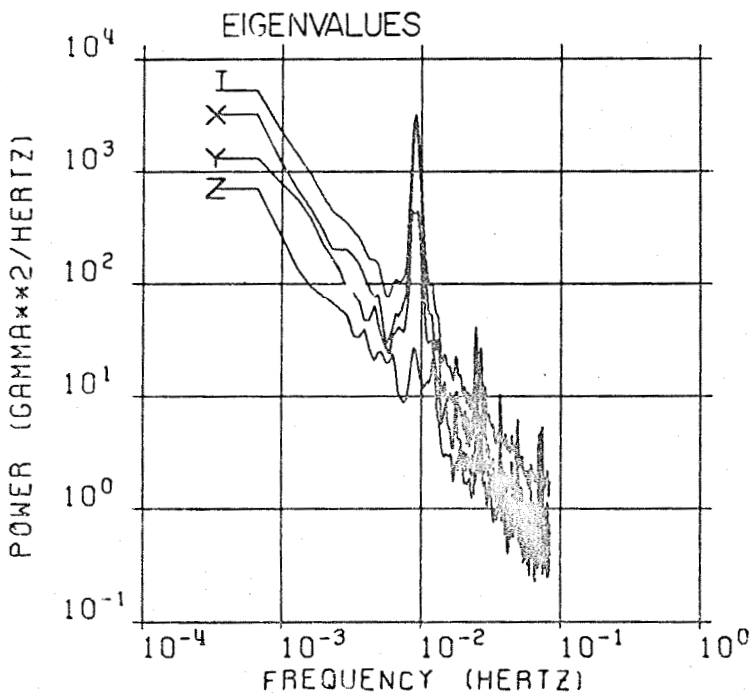

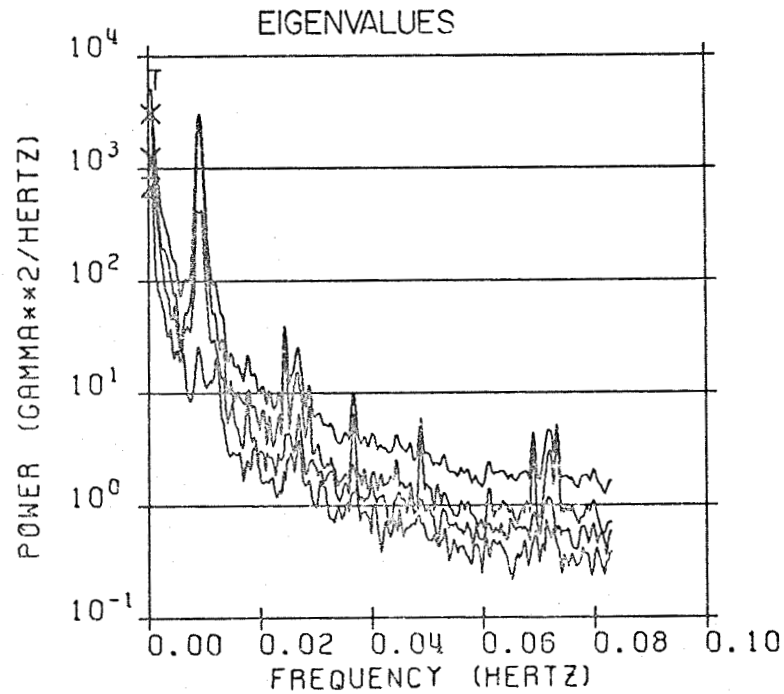

SPECTRAL ANALYSIS PARAMETERS

NPTS = 4096
DIGINT = 6.0 SECONDS
NDEG = 26
BNWDTH = .0005289
BNSEP = .0003255

POLARIZATION AND ELLIPTICITY

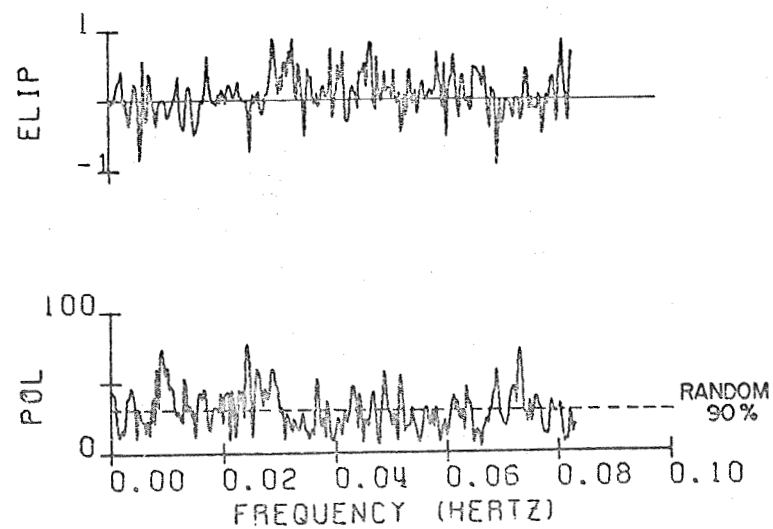

Figure 7

NOISE BURSTS
0808-0916 UT, OCT 10, 1969
UCLA ATS-1 MAGNETOMETER

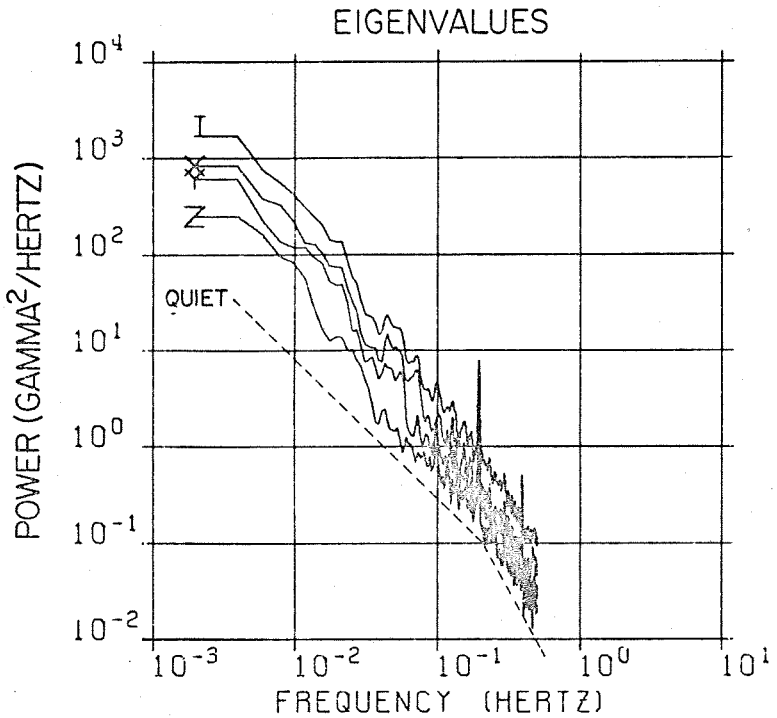

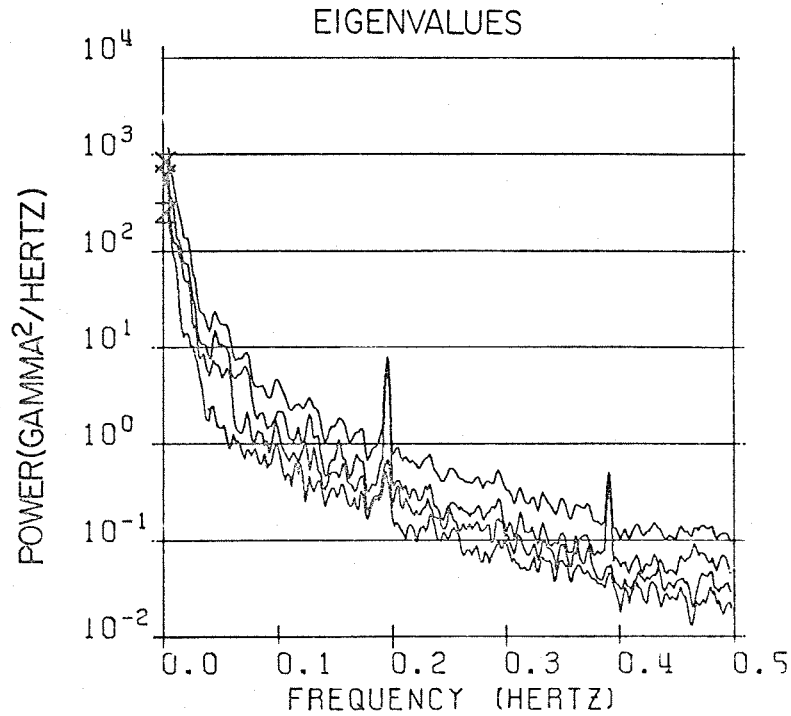

SPECTRAL ANALYSIS PARAMETERS

NPTS = 4096
DIGINT = 1.0 SECONDS
NDEG = 26
BNWDTH = .00317 HZ
BNSEP = .00195 HZ

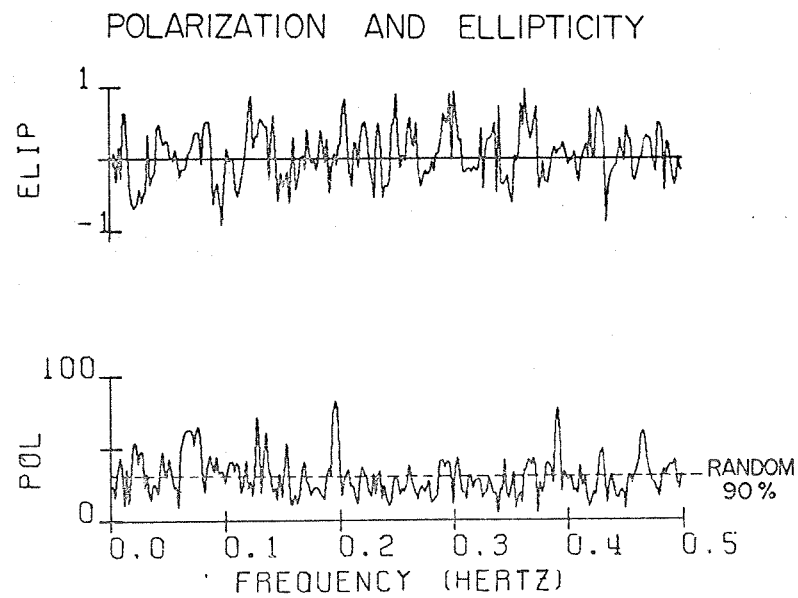

Figure 8

List of Tables

1. Table listing data recovered from UCLA magnetometer on ATS-1 since time of launch. Major events in the history of the spacecraft are indicated under remarks.

2. Correction vector for spacecraft field in eclipse zero modes at three successive equinoxes. An eclipse mode is defined as the state of the spacecraft at the time of eclipse. A zero mode is defined as a state in which a minimum number of subsystems is operating.

3. Segment of the listing of the ATS-1 spacecraft state vector including the interval of time displayed in Figure 2. The three right most columns are the components of the correction vector for the indicated state. The symbols 3333.3 indicate an unknown correction.

4. List of octal commands sent to ATS-1 during 1967 and 1968. A brief interpretation of this command is given in second columns.

5. Interpretation of ATS-1 state vector. The state vector is broken into three words of eight characters each. Each character is in hexadecimal.

6. Listing of ATS-1 states during 1967 and then 1968. During each year the states are ordered by decreasing total duration.

7. Format of corrected data tapes.

Table 1

ATS-1 Received Data Coverage, Monthly
(Estimates)

Yr	Mo	%	Remarks
1966	Dec.	30	Data starts Dec. 9, sporadic until 24th.
1967	Jan.	95	
	Feb.	90	
	Mar.	60	
	Apr.	70	
	May	75	
	Jun.	80	
	Jul.	90	
	Aug.	95	
	Sept.	95	
	Oct.	95	
	Nov.	75	
	Dec.	100	
1968	Jan.	98	
	Feb.	100	
	Mar.	75	
	Apr.	100	
	May	95	
	Jun.	95	
	Jul.	85	
	Aug.	70	UCLA OFF starging August 23
	Sept.	0	UCLA OFF all month
	Oct.	70	UCLA OFF until Oct. 8
	Nov.	85	
	Dec.	65	No data Dec. 19 thru 27, and 30, 31
1969	Jan.	50	Usually OFF 1400-2200, RSST OFF starting 24
	Feb.	50	Usually OFF 1400-2200, RSST OFF all month
	Mar.	40	RSST OFF to 9th, ON 10th to 21st; UCLA OFF 21
	Apr.	0	UCLA OFF all month
	May	15	UCLA OFF to 10th; ON 11 to 25, OFF from 26
	Jun.	25	No data 1400 - 2400 every day; RSST & UCLA ON
	Jul.	50	No data from 15th to 28th
	Aug.	80	
	Sept.	90	
	Oct.	45	No data from 14th to 28th
	Nov.	80	RSST OFF Nov. 2; processing halted
	Dec.		
1970	Jan.		
	Feb.		
	Mar.	80	Unprocessed; can only estimate coverage
	Apr.		by looking at DECOM listings; Goddard
	May		still sending tapes for this period.
	Jun.		
	Jul.		Goddard may have data; status unclear.
	Aug.		
	Sept.		
	Oct.	75	NOAA Boulder Coverage
	Nov.	90	
	Dec.	80	

Yr	Mo	%	Remarks
1971	Jan.	82	
	Feb.	83	
	Mar.	56	
	Apr.	85	
	May	85	
	Jun.	91	

Table 2

Correction Vector for Spacecraft Field
Comparison of Eclipse Zero Modes

	Spring 1967	Fall 1967	Spring 1968
CX	11.1±1	9.6±1	9.4±1
CY	22.8±1	22.3±1	22.7±1
CZ	82±7	89±8	90±6

Table 3

DATE = 67 078 MAR 19 ATS STATE LISTING 00/30/71 PAGE = 1

MICROWAVE SYSTEM#1	OFF		YEAR DAY MTH DY HH:MM:SS
MICROWAVE SYSTEM#1	F3ONHV		67 077 MAR 18 23:29:20
MICROWAVE POWER	PSDS ~~PCE4~~ PDE2		COM <--COMMAND INTERPRETATION-->
VHF REGULATORS	OFF		254 $SSCC SOUTH FRAME OVERRIDE
SPIN SCAN CLOUD CLOUD CAMERA	NORM		#MICRO1#|#MICRO2#|MVSTTEEE
TELEMETRY	TM#1 ~~TM#3~~ ~~TM#2~~ TM#4 ~~ENC1~~ ENC2 ~~EC4~~-S~~B02~~-		10000000|952400C5|50294D7F
EME POWER SUPPLY	PREG RLY1 ~~RLY2~~ PSUP		<-FLAG-> XXXX.X YYYY.Y ZZZZ.Z
EME EXPERIMENTS	UCLA RICE AERO SOLA MINN MMAG BTLB		00000001 11.6 15.8 118.9

HH:MM:SS	COM	<--COMMAND INTERPRETATION-->	#MICRO1#	#MICRO2#	VHF	SSCC	#MICRO1#	#MICRO2#	MVSTTEEE	<-FLAG->	XXXX.X	YYYY.Y	ZZZZ.Z
01:10:20	133	$SSCC REGULATOR OFF	OFF	F3ONHV	OFF	OFF	10000000	952400C5	50094D7F	00000001	11.5	18.1	114.6
01:10:50	270	#2 MICRO FT MODE ON	OFF	F3ONHV	OFF	OFF	10000000	C52400C5	50094D7F	00000001	11.5	18.1	114.6
01:58:35	374	#2 MICRO OFF	OFF	OFF	OFF	OFF	10000000	40000000	50094D7F	00000001	9.4	22.7	90.0
01:59:00	376	%VHF REGULATOR 1 ON	OFF	OFF	1	OFF	10000000	40000000	52094D7F	FFFFFFFF	3333.3	3333.3	3333.3
01:59:30	251	%VHF REGULATOR 2 ON	OFF	OFF	1&2	OFF	10000000	40000000	53094D7F	00000001	14.3	10.8	138.3
01:59:55	275	%VHF W/F GENERATOR 2 ON/OFF	OFF	OFF	1&2	OFF	10000000	40000000	53094D7F	00000001	14.3	10.8	138.3
02:25:45	302	%VHF REGULATOR 1 OFF	OFF	OFF	2	OFF	10000000	40000000	51094D7F	FFFFFFFF	3333.3	3333.3	3333.3
02:27:05	027	%VHF REGULATOR 2 OFF	OFF	OFF	OFF	OFF	10000000	40000000	50094D7F	00000001	9.4	22.7	90.0
02:27:30	275	%VHF W/F GENERATOR 2 ON/OFF	OFF	OFF	OFF	OFF	10000000	40000000	50094D7F	00000001	9.4	22.7	90.0
02:27:55	164	#2 MICRO TWT 3 FIL ON	OFF	F3	OFF	OFF	10000000	44440000	50094D7F	FFFFFFFF	3333.3	3333.3	3333.3
02:28:20	232	#2 MICRO TWT 4 FIL ON	OFF	F3F4	OFF	OFF	10000000	46444600	50094D7F	FFFFFFFF	3333.3	3333.3	3333.3
02:28:50	336	#2 MICRO MA MODE ON	OFF	F3F4ON	OFF	OFF	10000000	A6444600	50094D7F	FFFFFFFF	3333.3	3333.3	3333.3
02:32:20	126	#2 MICRO TWT HV ON	OFF	F3F4ONHV	OFF	OFF	10000000	A74446A7	50094D7F	00000001	12.6	15.7	125.4
03:04:25	270	#2 MICRO FT MODE ON	OFF	F3F4ONHV	OFF	OFF	10000000	C74446A7	50094D7F	00000001	12.6	15.7	125.4
03:18:30	374	#2 MICRO OFF	OFF	OFF	OFF	OFF	10000000	40000000	50094D7F	00000001	9.4	22.7	90.0
03:18:55	164	#2 MICRO TWT 3 FIL ON	OFF	F3	OFF	OFF	10000000	44440000	50094D7F	FFFFFFFF	3333.3	3333.3	3333.3
03:19:20	270	#2 MICRO FT MODE ON	OFF	F3ON	OFF	OFF	10000000	C4440000	50094D7F	FFFFFFFF	3333.3	3333.3	3333.3
03:22:55	126	#2 MICRO TWT HV ON	OFF	F3ONHV	OFF	OFF	10000000	C54400C5	50094D7F	00000001	11.5	18.1	114.6
03:23:20	232	#2 MICRO TWT 4 FIL ON	OFF	F3ONHVF4	OFF	OFF	10000000	C744C7C5	50094D7F	FFFFFFFF	3333.3	3333.3	3333.3
03:27:10	374	#2 MICRO OFF	OFF	OFF	OFF	OFF	10000000	40000000	50094D7F	00000001	9.4	22.7	90.0
03:27:30	232	#2 MICRO TWT 4 FIL ON	OFF	F4	OFF	OFF	10000000	42004200	50094D7F	FFFFFFFF	3333.3	3333.3	3333.3
03:28:00	270	#2 MICRO FT MODE ON	OFF	F4ON	OFF	OFF	10000000	C2004200	50094D7F	FFFFFFFF	3333.3	3333.3	3333.3
03:31:30	126	#2 MICRO TWT HV ON	OFF	F4ONHV	OFF	OFF	10000000	C30042C3	50094D7F	FFFFFFFF	3333.3	3333.3	3333.3
03:31:55	164	#2 MICRO TWT 3 FIL ON	OFF	F4ONHVF3	OFF	OFF	10000000	C7C742C3	50094D7F	FFFFFFFF	3333.3	3333.3	3333.3
03:35:35	374	#2 MICRO OFF	OFF	OFF	OFF	OFF	10000000	40000000	50094D7F	00000001	9.4	22.7	90.0
03:36:00	164	#2 MICRO TWT 3 FIL ON	OFF	F3	OFF	OFF	10000000	44440000	50094D7F	FFFFFFFF	3333.3	3333.3	3333.3
03:36:30	232	#2 MICRO TWT 4 FIL ON	OFF	F3F4	OFF	OFF	10000000	464446C0	50094D7F	FFFFFFFF	3333.3	3333.3	3333.3
03:36:55	270	#2 MICRO FT MODE ON	OFF	F3F4ON	OFF	OFF	10000000	C64446C0	50094D7F	FFFFFFFF	3333.3	3333.3	3333.3
03:40:00	126	#2 MICRO TWT HV ON	OFF	F3F4ONHV	OFF	OFF	10000000	C74446C7	50094D7F	00000001	12.6	15.7	125.4
03:44:45	066	@EME SOLAR CELL HALT/RESET	OFF	F3F4ONHV	OFF	OFF	10000000	C74446C7	50094D7F	00000001	12.6	15.7	125.4
04:01:20	336	#2 MICRO MA MODE ON	OFF	F3F4ONHV	OFF	OFF	10000000	A74446C7	50094D7F	00000001	12.6	15.7	125.4
04:53:30	374	#2 MICRO OFF	OFF	OFF	OFF	OFF	10000000	20000000	50094D7F	00000001	9.4	22.7	90.0
04:54:15	336	#2 MICRO MA MODE ON	OFF	ON	OFF	OFF	10000000	A0000000	50094D7F	FFFFFFFF	3333.3	3333.3	3333.3
04:54:45	164	#2 MICRO TWT 3 FIL ON	OFF	ONF3	OFF	OFF	10000000	A4A40000	50094D7F	00000001	10.0	21.5	102.4
04:58:45	126	#2 MICRO TWT HV ON	OFF	ONF3HV	OFF	OFF	10000000	A5A400A5	50094D7F	00000001	11.7	18.1	116.3
04:59:15	232	#2 MICRO TWT 4 FIL ON	OFF	ONF3HVF4	OFF	OFF	10000000	A7A4A7A5	50094D7F	FFFFFFFF	3333.3	3333.3	3333.3
05:03:35	374	#2 MICRO OFF	OFF	OFF	OFF	OFF	10000000	20000000	50094D7F	00000001	9.4	22.7	90.0
05:04:00	336	#2 MICRO MA MODE ON	OFF	ON	OFF	OFF	10000000	A0000000	50094D7F	FFFFFFFF	3333.3	3333.3	3333.3
05:04:25	232	#2 MICRO TWT 4 FIL ON	OFF	ONF4	OFF	OFF	10000000	A200A200	50094D7F	FFFFFFFF	3333.3	3333.3	3333.3
05:08:25	126	#2 MICRO TWT HV ON	OFF	ONF4HV	OFF	OFF	10000000	A300A2A3	50094D7F	FFFFFFFF	3333.3	3333.3	3333.3
05:09:15	164	#2 MICRO TWT 3 FIL ON	OFF	ONF4HVF3	OFF	OFF	10000000	A7A7A2A3	50094D7F	FFFFFFFF	3333.3	3333.3	3333.3
05:13:40	374	#2 MICRO OFF	OFF	OFF	OFF	OFF	10000000	20000000	50094D7F	00000001	9.4	22.7	90.0
05:14:05	270	#2 MICRO FT MODE ON	OFF	ON	OFF	OFF	10000000	C0000000	50094D7F	FFFFFFFF	3333.3	3333.3	3333.3
05:14:30	164	#2 MICRO TWT 3 FIL ON	OFF	ONF3	OFF	OFF	10000000	C4C40000	50094D7F	00000001	10.0	21.5	102.4
05:18:30	126	#2 MICRO TWT HV ON	OFF	ONF3HV	OFF	OFF	10000000	C5C400C5	50094D7F	00000001	11.7	18.1	116.3
08:08:30	060	#2 MICRO WBD MODE ON	OFF	ONF3HV	OFF	OFF	10000000	95C400C5	50094D7F	00000001	11.7	18.1	116.3
08:08:55	006	$SSCC REGULATOR ON	OFF	ONF3HV	OFF	NORM	10000000	95C400C5	50294D7F	00000001	13.3	16.7	120.9
08:09:20	066	@EME SOLAR CELL HALT/RESET	OFF	ONF3HV	OFF	NORM	10000000	95C400C5	50294D7F	00000001	13.3	16.7	120.9

MICROWAVE SYSTEM#1	OFF												
MICROWAVE SYSTEM#1	ONF3HV												
MICROWAVE POWER	PSDS PE84 PDE2												
VHF REGULATORS	OFF												
SPIN SCAN CLOUD CLOUD CAMERA	NORM												
TELEMETRY	TM#1 TM#3 TM#2 TM#4 ENC4 ENC2 E04-SEC 2-												
EME POWER SUPPLY	PREG RLY1 RLY2 PSUP												
EME EXPERIMENTS	UCLA RICE AERO SOLA MINN MMAG BTLB												

YEAR DAY MTH DY	HH:MM:SS
67 078 MAR 19	08:09:20

COM <--COMMAND INTERPRETATION-->			
066 @EME SOLAR CELL HALT/RESET			
#MICRO1#	#MICRO2#	MVSTTEEE	
10000000	95C400C5	50294D7F	
<-FLAG->	XXXX.X	YYYY.Y	ZZZZ.Z
00000001	13.3	16.7	120.9

HH:MM:SS	COM	<--COMMAND INTERPRETATION-->	#MICRO1#	#MICRO2#	VHF	SSCC	#MICRO1#	#MICRO2#	MVSTTEEE	<-FLAG->	XXXX.X	YYYY.Y	ZZZZ.Z
08:10:30	020	-MISC ACCUMULATOR SELECT A	OFF	ONF3HV	OFF	NORM	10000000	95C400C5	50294D7F	00000001	13.3	16.7	120.9
08:23:00	254	$SSCC SOUTH FRAME OVERRIDE	OFF	ONF3HV	OFF	NORM	10000000	95C400C5	50294D7F	00000001	13.3	16.7	120.9
08:34:50	133	$SSCC REGULATOR OFF	OFF	ONF3HV	OFF	OFF	10000000	95C400C5	50094D7F	00000001	11.7	18.1	116.3
08:35:20	271	*TM SCO 1 ON (W/F ON)	OFF	ONF3HV	OFF	OFF	10000000	95C400C5	50096D7F	00000001	11.7	18.1	116.3
08:41:55	131	#2 MICRO WBD MODE SELECT	OFF	ONF3HV	OFF	OFF	10000000	95C400C5	50096D7F	00000001	11.7	18.1	116.3
09:20:00	103	@EME ECLIPSE MODE ON	OFF	ONF3HV	OFF	OFF	10000000	95C400C5	50096D7F	00000001	11.7	18.1	116.3
10:48:30	224	@EME ECLIPSE MODE OFF	OFF	ONF3HV	OFF	OFF	10000000	95C400C5	50096D7F	00000001	11.7	18.1	116.3
10:52:00	316	*TM SCO 1 OFF,2 OFF	OFF	ONF3HV	OFF	OFF	10000000	95C400C5	50094D7F	00000001	11.7	18.1	116.3
10:56:10	374	#2 MICRO OFF	OFF	OFF	OFF	OFF	10000000	10000000	50094D7F	00000001	9.4	22.7	90.0
10:56:55	376	%VHF REGULATOR 1 ON	OFF	OFF	1	OFF	10000000	10000000	52094D7F	FFFFFFFF	3333.3	3333.3	3333.3
10:57:30	251	%VHF REGULATOR 2 ON	OFF	OFF	1&2	OFF	10000000	10000000	53094D7F	00000001	14.3	10.8	138.3
10:57:55	275	%VHF W/F GENERATOR 2 ON/OFF	OFF	OFF	1&2	OFF	10000000	10000000	53094D7F	00000001	14.3	10.8	138.3
11:59:45	270	#2 MICRO FT MODE ON	OFF	ON	1&2	OFF	10000000	C0000000	53094D7F	FFFFFFFF	3333.3	3333.3	3333.3
12:00:15	164	#2 MICRO TWT 3 FIL ON	OFF	ONF3	1&2	OFF	10000000	C4C40000	53094D7F	FFFFFFFF	3333.3	3333.3	3333.3
12:00:45	302	%VHF REGULATOR 1 OFF	OFF	ONF3	2	OFF	10000000	C4C40000	51094D7F	FFFFFFFF	3333.3	3333.3	3333.3
12:01:10	027	%VHF REGULATOR 2 OFF	OFF	ONF3	OFF	OFF	10000000	C4C40000	50094D7F	00000001	10.0	21.5	102.4
12:01:40	275	%VHF W/F GENERATOR 2 ON/OFF	OFF	ONF3	OFF	OFF	10000000	C4C40000	50094D7F	00000001	10.0	21.5	102.4
12:02:05	066	@EME SOLAR CELL HALT/RESET	OFF	ONF3	OFF	OFF	10000000	C4C40000	50094D7F	00000001	10.0	21.5	102.4
12:04:15	126	#2 MICRO TWT HV ON	OFF	ONF3HV	OFF	OFF	10000000	C5C400C5	50094D7F	00000001	11.7	18.1	116.3
12:10:50	374	#2 MICRO OFF	OFF	OFF	OFF	OFF	10000000	40000000	50094D7F	00000001	9.4	22.7	90.0
12:11:15	376	%VHF REGULATOR 1 ON	OFF	OFF	1	OFF	10000000	40000000	52094D7F	FFFFFFFF	3333.3	3333.3	3333.3
12:11:40	251	%VHF REGULATOR 2 ON	OFF	OFF	1&2	OFF	10000000	40000000	53094D7F	00000001	14.3	10.8	138.3
12:12:05	275	%VHF W/F GENERATOR 2 ON/OFF	OFF	OFF	1&2	OFF	10000000	40000000	53094D7F	00000001	14.3	10.8	138.3
13:39:10	275	%VHF W/F GENERATOR 2 ON/OFF	OFF	OFF	1&2	OFF	10000000	40000000	53094D7F	00000001	14.3	10.8	138.3
13:47:40	302	%VHF REGULATOR 1 OFF	OFF	OFF	2	OFF	10000000	40000000	51094D7F	FFFFFFFF	3333.3	3333.3	3333.3
13:48:40	027	%VHF REGULATOR 2 OFF	OFF	OFF	OFF	OFF	10000000	40000000	50094D7F	00000001	9.4	22.7	90.0
13:49:25	164	#2 MICRO TWT 3 FIL ON	OFF	F3	OFF	OFF	10000000	44440000	50094D7F	FFFFFFFF	3333.3	3333.3	3333.3
13:49:50	232	#2 MICRO TWT 4 FIL ON	OFF	F3F4	OFF	OFF	10000000	46444600	50094D7F	FFFFFFFF	3333.3	3333.3	3333.3
13:50:15	270	#2 MICRO FT MODE ON	OFF	F3F4ON	OFF	OFF	10000000	C6444600	50094D7F	FFFFFFFF	3333.3	3333.3	3333.3
13:54:15	126	#2 MICRO TWT HV ON	OFF	F3F4ONHV	OFF	OFF	10000000	C74446C7	50094D7F	00000001	12.6	15.7	125.4
14:28:25	374	#2 MICRO OFF	OFF	OFF	OFF	OFF	10000000	40000000	50094D7F	00000001	9.4	22.7	90.0
14:29:00	164	#2 MICRO TWT 3 FIL ON	OFF	F3	OFF	OFF	10000000	44440000	50094D7F	FFFFFFFF	3333.3	3333.3	3333.3
14:29:30	270	#2 MICRO FT MODE ON	OFF	F3ON	OFF	OFF	10000000	C4440000	50094D7F	FFFFFFFF	3333.3	3333.3	3333.3
14:33:00	126	#2 MICRO TWT HV ON	OFF	F3ONHV	OFF	OFF	10000000	C54400C5	50094D7F	00000001	11.5	18.1	114.6
14:33:30	232	#2 MICRO TWT 4 FIL ON	OFF	F3ONHVF4	OFF	OFF	10000000	C744C7C5	50094D7F	FFFFFFFF	3333.3	3333.3	3333.3
14:37:00	374	#2 MICRO OFF	OFF	OFF	OFF	OFF	10000000	40000000	50094D7F	00000001	9.4	22.7	90.0
14:37:30	232	#2 MICRO TWT 4 FIL ON	OFF	F4	OFF	OFF	10000000	42004200	50094D7F	FFFFFFFF	3333.3	3333.3	3333.3
14:38:00	270	#2 MICRO FT MODE ON	OFF	F4ON	OFF	OFF	10000000	C2004200	50094D7F	FFFFFFFF	3333.3	3333.3	3333.3
14:41:30	126	#2 MICRO TWT HV ON	OFF	F4ONHV	OFF	OFF	10000000	C30042C3	50094D7F	FFFFFFFF	3333.3	3333.3	3333.3
14:42:00	164	#2 MICRO TWT 3 FIL ON	OFF	F4ONHVF3	OFF	OFF	10000000	C7C742C3	50094D7F	FFFFFFFF	3333.3	3333.3	3333.3
14:46:15	374	#2 MICRO OFF	OFF	OFF	OFF	OFF	10000000	40000000	50094D7F	00000001	9.4	22.7	90.0
14:49:00	164	#2 MICRO TWT 3 FIL ON	OFF	F3	OFF	OFF	10000000	44440000	50094D7F	FFFFFFFF	3333.3	3333.3	3333.3
14:49:30	060	#2 MICRO WBD MODE ON	OFF	F3ON	OFF	OFF	10000000	94440000	50094D7F	FFFFFFFF	3333.3	3333.3	3333.3
14:53:00	126	#2 MICRO TWT HV ON	OFF	F3ONHV	OFF	OFF	10000000	95440095	50094D7F	00000001	11.5	18.1	114.6
14:54:30	270	#2 MICRO FT MODE ON	OFF	F3ONHV	OFF	OFF	10000000	C5440095	50094D7F	00000001	11.5	18.1	114.6
14:55:00	232	#2 MICRO TWT 4 FIL ON	OFF	F3ONHVF4	OFF	OFF	10000000	C744C795	50094D7F	FFFFFFFF	3333.3	3333.3	3333.3
14:58:35	374	#2 MICRO OFF	OFF	OFF	OFF	OFF	10000000	40000000	50094D7F	00000001	9.4	22.7	90.0
14:59:05	232	#2 MICRO TWT 4 FIL ON	OFF	F4	OFF	OFF	10000000	42004200	50094D7F	FFFFFFFF	3333.3	3333.3	3333.3

MICROWAVE SYSTEM#1	OFF	YEAR DAY MTH DY HH:MM:SS
MICROWAVE SYSTEM#1	F4	67 078 MAR 19 14:59:05
MICROWAVE POWER	PSDS PCB4 PDE2	COM <--COMMAND INTERPRETATION-->
VHF REGULATORS	OFF	232 #2 MICRO TWT 4 FIL ON
SPIN SCAN CLOUD CLOUD CAMERA	OFF	#MICRO1#|#MICRO2#|MVSTTEEE
TELEMETRY	TM#1 TM#3 TM#2 TM#4 ENC4 ENC2 C04-SBO2-	10000000|42004200|50094D7F
EME POWER SUPPLY	PREG RLY1 RLY2 PSUP	<-FLAG-> XXXX.X YYYY.Y ZZZZ.Z
EME EXPERIMENTS	UCLA RICE AERO SOLA MINN MMAG BTLB	FFFFFFFF 3333.3 3333.3 3333.3

HH:MM:SS	COM	<--COMMAND INTERPRETATION-->	#MICRO1#	#MICRO2#	VHF	SSCC	#MICRO1#	#MICRO2#	MVSTTEEE	<-FLAG->	XXXX.X	YYYY.Y	ZZZZ.Z
14:59:30	270	#2 MICRO FT MODE ON	OFF	F4ON	OFF	OFF	10000000	C2004200	50094D7F	FFFFFFFF	3333.3	3333.3	3333.3
15:03:05	126	#2 MICRO TWT HV ON	OFF	F4ONHV	OFF	OFF	10000000	C30042C3	50094D7F	FFFFFFFF	3333.3	3333.3	3333.3
15:03:30	164	#2 MICRO TWT 3 FIL ON	OFF	F4ONHVF3	OFF	OFF	10000000	C7C742C3	50094D7F	FFFFFFFF	3333.3	3333.3	3333.3
15:07:15	374	#2 MICRO OFF	OFF	OFF	OFF	OFF	10000000	40000000	50094D7F	00000001	9.4	22.7	90.0
15:07:45	164	#2 MICRO TWT 3 FIL ON	OFF	F3	OFF	OFF	10000000	44440000	50094D7F	FFFFFFFF	3333.3	3333.3	3333.3
15:08:15	060	#2 MICRO WBD MODE ON	OFF	F3ON	OFF	OFF	10000000	94440000	50094D7F	FFFFFFFF	3333.3	3333.3	3333.3
15:11:45	126	#2 MICRO TWT HV ON	OFF	F3ONHV	OFF	OFF	10000000	95440095	50094D7F	00000001	11.5	18.1	114.6
15:12:15	006	$SSCC REGULATOR ON	OFF	F3ONHV	OFF	NORM	10000000	95440095	50294D7F	00000001	11.6	15.8	118.9
16:04:25	254	$SSCC SOUTH FRAME OVERRIDE	OFF	F3ONHV	OFF	NORM	10000000	95440095	50294D7F	00000001	11.6	15.8	118.9
16:14:00	254	$SSCC SOUTH FRAME OVERRIDE	OFF	F3ONHV	OFF	NORM	10000000	95440095	50294D7F	00000001	11.6	15.8	118.9
16:18:00	254	$SSCC SOUTH FRAME OVERRIDE	OFF	F3ONHV	OFF	NORM	10000000	95440095	50294D7F	00000001	11.6	15.8	118.9
16:35:20	254	$SSCC SOUTH FRAME OVERRIDE	OFF	F3ONHV	OFF	NORM	10000000	95440095	50294D7F	00000001	11.6	15.8	118.9
17:16:50	020	-MISC ACCUMULATOR SELECT A	OFF	F3ONHV	OFF	NORM	10000000	95440095	50294D7F	00000001	11.6	15.8	118.9
17:37:00	254	$SSCC SOUTH FRAME OVERRIDE	OFF	F3ONHV	OFF	NORM	10000000	95440095	50294D7F	00000001	11.6	15.8	118.9
17:43:00	254	$SSCC SOUTH FRAME OVERRIDE	OFF	F3ONHV	OFF	NORM	10000000	95440095	50294D7F	00000001	11.6	15.8	118.9
19:07:10	066	@EME SOLAR CELL HALT/RESET	OFF	F3ONHV	OFF	NORM	10000000	95440095	50294D7F	00000001	11.6	15.8	118.9
19:19:50	254	$SSCC SOUTH FRAME OVERRIDE	OFF	F3ONHV	OFF	NORM	10000000	95440095	50294D7F	00000001	11.6	15.8	118.9
19:50:00	254	$SSCC SOUTH FRAME OVERRIDE	OFF	F3ONHV	OFF	NORM	10000000	95440095	50294D7F	00000001	11.6	15.8	118.9
20:07:50	254	$SSCC SOUTH FRAME OVERRIDE	OFF	F3ONHV	OFF	NORM	10000000	95440095	50294D7F	00000001	11.6	15.8	118.9
21:15:10	254	$SSCC SOUTH FRAME OVERRIDE	OFF	F3ONHV	OFF	NORM	10000000	95440095	50294D7F	00000001	11.6	15.8	118.9
21:16:05	254	$SSCC SOUTH FRAME OVERRIDE	OFF	F3ONHV	OFF	NORM	10000000	95440095	50294D7F	00000001	11.6	15.8	118.9
21:52:20	133	$SSCC REGULATOR OFF	OFF	F3ONHV	OFF	OFF	10000000	95440095	50094D7F	00000001	11.5	18.1	114.6
21:59:30	374	#2 MICRO OFF	OFF	OFF	OFF	OFF	10000000	10000000	50094D7F	00000001	9.4	22.7	90.0
21:59:50	376	%VHF REGULATOR 1 ON	OFF	OFF	1	OFF	10000000	10000000	52094D7F	FFFFFFFF	3333.3	3333.3	3333.3
22:00:10	251	%VHF REGULATOR 2 ON	OFF	OFF	1&2	OFF	10000000	10000000	53094D7F	00000001	14.3	10.8	138.3
22:00:45	275	%VHF W/F GENERATOR 2 ON/OFF	OFF	OFF	1&2	OFF	10000000	10000000	53094D7F	00000001	14.3	10.8	138.3
22:27:20	302	%VHF REGULATOR 1 OFF	OFF	OFF	2	OFF	10000000	10000000	51094D7F	FFFFFFFF	3333.3	3333.3	3333.3
22:27:50	027	%VHF REGULATOR 2 OFF	OFF	OFF	OFF	OFF	10000000	10000000	50094D7F	00000001	9.4	22.7	90.0
22:28:20	275	%VHF W/F GENERATOR 2 ON/OFF	OFF	OFF	OFF	OFF	10000000	10000000	50094D7F	00000001	9.4	22.7	90.0
22:29:00	060	#2 MICRO WBD MODE ON	OFF	ON	OFF	OFF	10000000	90000000	50094D7F	FFFFFFFF	3333.3	3333.3	3333.3
22:29:25	164	#2 MICRO TWT 3 FIL ON	OFF	ONF3	OFF	OFF	10000000	94940000	50094D7F	00000001	10.0	21.5	102.4
22:30:45	270	#2 MICRO FT MODE ON	OFF	ONF3	OFF	OFF	10000000	C4940000	50094D7F	00000001	10.0	21.5	102.4
22:33:40	126	#2 MICRO TWT HV ON	OFF	ONF3HV	OFF	OFF	10000000	C59400C5	50094D7F	00000001	11.7	18.1	116.3
22:43:35	060	#2 MICRO WBD MODE ON	OFF	ONF3HV	OFF	OFF	10000000	959400C5	50094D7F	00000001	11.7	18.1	116.3
22:44:05	006	$SSCC REGULATOR ON	OFF	ONF3HV	OFF	NORM	10000000	959400C5	50294D7F	00000001	13.3	16.7	120.9
22:46:00	340	$SSCC NORMAL SCAN	OFF	ONF3HV	OFF	NORM	10000000	959400C5	50294D7F	00000001	13.3	16.7	120.9
22:57:55	254	$SSCC SOUTH FRAME OVERRIDE	OFF	ONF3HV	OFF	NORM	10000000	959400C5	50294D7F	00000001	13.3	16.7	120.9

Table 4

LISTING OF INTERPRETATION OF ATS OCTAL COMMANDS

COM	COMMAND INTERPRETATION
001	#1 MICRO TWT HV ON
002	*TM PCM ENCODER 1 ON
003	*TM TRANSMITTER 4 ON,2 OFF
004	#1 MICRO WBD MODE SELECT
006	$SSCC REGULATOR ON
007	@EME UCLA OFF
013	+ORIENT THRUST 2 OFF
016	*TM PCM ENCODER SELECT WBD63
017	-MISC ANGLE CENTER MODE SLCT
020	-MISC ACCUMULATOR SELECT A
022	#1 MICRO TWT 1 FIL ON
023	*TM TRANSMITTER 2 OFF,4 OFF
024	@EME EXP POWER SUPPLY ON X
025	@EME BTL BIAS OFF
027	%VHF REGULATOR 2 OFF
034	%VHF W/F SWITCH 1 ON/OFF
040	*TM SCO 1 ON
046	@EME RICE ON
051	+ORIENT THRUST 1 OFF
060	#2 MICRO WBD MODE ON
061	*TM PCM ENCODER 2 SELECT
065	$SSCC BACK-TO-BACK SCAN
066	@EME SOLAR CELL HALT/RESET
076	# MICRO PACE 1 ON,2 OFF
077	*TM PCM ENCODER 2 OFF
101	+ORIENT FIRE APOGEE MOTOR
103	@EME ECLIPSE MODE ON
106	*TM PCM ENCODER SELECT WRD_
107	-MISC SOLAR ARRAY UNPARALLEL
110	@EME RICE OFF
113	@EME UNIV OF MINN ON
120	# MICRO ANTENNA POSITIVE
124	+ORIENT NUTATION REG ON
125	@EME REGULATOR OFF
126	#2 MICRO TWT HV ON
127	*TM PCM ENCODER 2 ON
130	@EME EXP BUS POWER ON ALT1
131	#2 MICRO WBD MODE SELECT
133	$SSCC REGULATOR OFF
141	# MICRO PSD ON
144	*TM TRANSMITTER 3 ON,1 OFF
147	#1 MICRO FT MODE ON
150	%VHF W/F GENERATOR 1 ON/OFF
151	@EME EXP POWER SUPPLY OFF X
152	@EME BTL BIAS ON
164	#2 MICRO TWT 3 FIL ON
165	*TM TRNSMTTR 1 ENCDR SELECT
172	@EME UNIV OF MINN MAG OFF
173	@EME AEROSPACE OFF
376	%VHF REGULATOR 1 ON

COM	COMMAND INTERPRETATION
176	+ORIENT THRUST 1 ON
203	+ORIENT RESISTO JET REG ON
207	# MICRO PSD OFF
210	+ORIENT FIRE RADIAL JET 1
211	#1 MICRO MA MODE ON
212	*TM TRANSMITTER 2 ON,4 OFF
217	*TM SCO 2 ON
224	@EME ECLIPSE MODE OFF
230	+ORIENT NUTATION REG OFF
232	#2 MICRO TWT 4 FIL ON
233	*TM TRNSMTTR 2 ENCDR SELECT
234	@EME SOLAR CELL ON
235	@EME EXP BUS POWER ON ALT2
245	# MICRO PACE 2 ON,1 OFF
250	*TM PCM ENCODER 1 OFF
251	%VHF REGULATOR 2 ON
253	#1 MICRO OFF
254	$SSCC SOUTH FRAME OVERRIDE
255	@EME UNIV OF MINN MAG ON
256	@EME AEROSPACE ON
270	#2 MICRO FT MODE ON
271	*TM SCO 1 ON (W/F ON)
273	+ORIENT FIRE AXIAL JET 1
275	%VHF W/F GENERATOR 2 ON/OFF
276	@EME EXP POWER SUPPLY OFF
277	@EME BTL BIAS ON X
300	@EME BTL BIAS-OFF ENABLE
302	%VHF REGULATOR 1 OFF
303	@EME EXP POWER SUPPLY ON
313	# MICRO PACE 1 OFF,2 OFF
315	#1 MICRO TWT 2 FIL ON
316	*TM SCO 1 OFF,2 OFF
324	+ORIENT RESISTO JET REG OFF
330	%VHF W/F SWITCH 2 ON/OFF
334	-MISC SOLAR ARRAY PARALLEL
335	+ORIENT FIRE AXIAL JET 2
336	#2 MICRO MA MODE ON
337	*TM PCM ENCODER 1 SELECT
340	$SSCC NORMAL SCAN
341	@EME UCLA ON
345	+ORIENT THRUST 2 ON
354	*TM TRANSMITTER 1 OFF,3 OFF
355	@EME REGULATOR ON
356	+ORIENT FIRE RADIAL JET 2
357	#1 MICRO WBD MODE ON
361	$SSCC NORTH FRAME OVERRIDE
362	@EME SOLAR CELL OFF
374	#2 MICRO OFF
375	*TM TRANSMITTER 1 ON,3 OFF

Table 5

State Descriptor Words

Word 1	Word 2	Word 3
1 2 3 4 5 6 7 8	1 2 3 4 5 6 7 8	1 2 3 4 5 6 7 8

Word 1 = Micro 1 Subsystem

1) 1 WB MODE, MICRO 1 OFF
   2 MA MODE, MICRO 1 OFF
4) 4 FT MODE, MICRO 1 OFF
   9 WB MODE, MICRO 1 ON
   A MA MODE, MICRO 1 ON
C) C FT MODE, MICRO 1 ON

2) 0 ALL OFF
   1 HIGH VOLTAGE ON
   2 FILAMENT 2 ON
   3 F2 & HV ON
   4 FILAMENT 1 ON
   5 F1 & HV ON
   6 F1 & F2 ON
   7 F1, F2, & HV ON

3) MICRO 1 MODE AFTER F1 TURNED ON
4) MICRO 1 SUBSYSTEMS AFTER F1 TURNED ON

5) MICRO 1 MODE AFTER F2 TURNED ON
6) MICRO 1 SUBSYSTEMS AFTER F2 TURNED ON

7) MICRO 1 MODE AFTER HV TURNED ON
8) MICRO 1 SUBSYSTEMS AFTER HV TURNED ON

WORD 2 = MICRO 2 SUBSYSTEM

1) Ø ALL OFF
   1 PACE 2 ON
   2 PACE 1 ON
   3 PACE 1, PACE 2 ON
   4 PSDS ON
   5 PSDS & PACE 2 ON
   6 PSDS & PACE 1 ON
   7 PSDS, PACE 1 & PACE 2 ON

MICRO SUPPLY

2) Ø ALL OFF
   1 VHF 2 ON
   2 VHF 1 ON
   3 VHF 1 & VHF 2 ON

VHF REGULATORS

Table 5, Continued

3)	Ø OFF, NORMAL SCAN 1 OFF, BACK-TO-BACK SCAN 2 ON, NORMAL SCAN 3 ON, BACK-TO-BACK SCAN	SSCC
4)	Ø ALL OFF 1 TM 4 ON 2 TM 2 ON 4 TM 3 ON 5 TM 3 & TM 4 ON 6 TM 2 & TM 3 ON 8 TM 1 ON 9 TM 1 & TM 4 ON A TM 1 & TM 2 ON	TELEMETRY
5)	Ø ALL OFF 1 SCO 2 ON 2 SCO 1 ON 4 ENC 2 ON 5 ENC 2 & SCO 2 ON 6 ENC 2 & SCO 1 ON 8 ENC 1 ON 9 SCO 2 & ENC1 ON A SCO 1 & ENC1 ON B 8+2+1 D=8+4+1 C = 8+4	.ENCODERS & .SCO
6)	Ø ALL OFF 1 PSUP 2 RLY2 3 RLY2, PSUP 4 RLY1 5 RLY1, PSUP 6 RLY1, RLY2 7 RLY1, RLY2, PSUP 8 PREG 9 PREG, PSUP A PREG, RLY2 B PREG, RLY2, PSUP C PREG, RLY1 D PREG, RLY1 PSUP E PREG, RLY1, RLY2 F PREG, RLY1, RLY2, PSUP	EME POWER
7)	Ø OFF 1 AERO 2 RICE 3 = 2+1 4 UCLA 5 = 4+1 6 = 4+2 7 = 4+2+1	EME EXPERIMENTS UCLA RICE AEROJET

Table 5, Continued

8)	Ø OFF	9 = 8+1	
	1 BTLB	A = 8+2	
	2 MMAG	B = 8+2+1	
	3 = 2+1	C = 8+4	
	4 MINN	D = 8+4+1	SOLAR EXPERIMENT
	5 = 4+1	E = 8+4+2	MINNESOTA
	6 = 4+2	F = 8+4+2+1	MINNESOTA MAGN
	7 = 4+2+1		BTLB
	9 SOLA		

Table 6

00000000	00000000	50060D00	44.81%
00000000	00000000	53060D00	9.49%
87848687	00000000	50060D00	9.33%
00000000	85840085	50260D00	6.94%
00000000	87848687	50060D00	5.70%
85840085	00000000	50060D00	2.52%
00000000	85840085	50060D00	2.41%
00000000	00000000	50020000	1.67%
00000000	00000000	50060C00	1.08%
87848687	85840085	50260D00	0.87%
85840085	85840085	50060D00	0.78%
00000000	83008283	50260D00	0.57%
00000000	00000000	53020000	0.56%
87848687	00000000	53060D00	0.47%
00000000	00000000	51060D00	0.44%
87848687	87848687	50060D00	0.37%
00000000	85040085	50260D00	0.37%
00000000	84840000	50060D00	0.36%
00000000	00000000	53060C00	0.36%
00000000	00000000	500A0000	0.36%
87848687	85840085	50060D00	0.35%
00000000	00000000	530A0000	0.33%
00000000	87848687	53060D00	0.33%
87848687	00000000	50020000	0.33%
00000000	85840085	53060D00	0.33%
87040687	00000000	50060D00	0.32%
00000000	85840085	50220000	0.30%
85840085	85840085	50260D00	0.30%
84840000	00000000	50060D00	0.29%
00000000	00000000	50060D00	0.28%
85840085	00000000	53060D00	0.27%
00000000	85840085	53260D00	0.27%
83008283	00000000	50060D00	0.26%
00000000	87848687	50260D00	0.25%
07010B08	00050007	052F0100	0.24%
85840085	00000000	50020000	0.22%
87048687	00000000	50060D00	0.22%
00000000	85840085	50260C00	0.21%
00000000	00000000	52060D00	0.20%
80000000	00000000	50060C00	0.19%
00000000	84840000	50260D00	0.15%
87848687	00000000	50060C00	0.15%
87040687	85840085	50060D00	0.14%
87848687	80000000	50060D00	0.14%
86848600	00000000	50060D00	0.14%
00000000	85040085	50060D00	0.13%
00000000	86848600	50060D00	0.13%
80000000	00000000	50020000	0.13%
85840085	87848687	50060D00	0.12%
00000000	83008283	50060D00	0.12%
00000000	87040687	50060D00	0.11%
80000000	00000000	50060D00	0.11%
87848687	85840085	50220000	0.10%
00000000	85840085	52060D00	0.09%
00000000	85840085	500A0000	0.09%
83008283	00000000	50020000	0.08%

Table 6 (con't)

82008200	00000000	50060D00	0.07%
00000000	82008200	50060D00	0.07%
80000000	00000000	53060C00	0.07%
87040687	00000000	50020D00	0.07%
00000000	00000000	50260D00	0.06%
85840085	00000000	52060D00	0.06%
85840085	00000000	50260D00	0.05%
00000000	87848785	50060D00	0.05%
84840000	00000000	53060D00	0.05%
00000000	87878283	50060D00	0.05%
87848687	83008283	50260D00	0.05%
87848687	00000000	53020000	0.05%
00000000	87848687	51060D00	0.05%
87848687	00000000	52060C00	0.05%
00000000	87848687	500A0000	0.05%
87848687	00000000	52020000	0.05%
87848687	00000000	52060D00	0.05%
87848785	00000000	50060D00	0.05%
00000000	80000000	53060D00	0.05%
87878283	00000000	50060D00	0.04%
00000000	84840000	53060D00	0.04%
00000000	85840085	51260D00	0.04%
87848687	00000000	51060D00	0.04%
87048687	85840085	50260D00	0.04%
87040687	81000081	50260D00	0.04%
85040085	00000000	50060000	0.04%
87040687	00000000	53060D00	0.04%
87848687	00000000	53060C00	0.04%
00000000	00000000	50260C00	0.04%
85840085	85840085	500A0000	0.04%
84840000	85840085	50260D00	0.04%
87848687	83008283	50260C00	0.04%
00000000	00000000	53000000	0.03%
00000000	85040085	53060D00	0.03%
85840085	00000000	500A0000	0.03%
85840085	85840085	53060D00	0.03%
00000000	81000081	50260D00	0.03%
00000000	83008283	53260D00	0.03%
00000000	85840085	51060D00	0.03%
84840000	00000000	50020000	0.03%
86848600	85840085	50260D00	0.03%
00000000	85040085	53260D00	0.03%
85840085	00000000	53020000	0.03%
00000000	87848687	52060D00	0.03%
00000000	87868287	50060D00	0.03%
87848687	84840000	50060D00	0.02%
85840085	85840085	50220000	0.02%
00000000	00000000	52020000	0.02%
87868700	80000000	50060D00	0.02%
00000000	87848687	50060C00	0.02%
80000000	00000000	53020000	0.02%
00000000	86848600	53060D00	0.02%
00000000	85840085	502A0000	0.02%
87848687	00000000	50260D00	0.02%
86808684	00000000	50060D00	0.02%
00000000	85840085	50020000	0.02%
87040687	85840085	50260D00	0.02%

Table 7
Format of ATS Leveled Data

This data will be printed on 7-track, BCD, 556 BPI tracks with record length of 132 characters, 20 records to the block.

Columns		Example	Explanation
02-03	Year	67	Time of Mid point of average
04-06	Day	014	
08-09	Hour	11	
10-11	Minute	38	
12-15	Second	07.5	
17-22	V	-6.8[1]	VDH Rotational System
23-28	D	10.2	
29-34	H	79.1	
35-40	V	-7.1[1]	VDH Dipole System
41-46	D	-5.4	
47-52	H	79.3	
53-58	X	-1.1 [1]	Uncorrected XYZ System
59-64	Y	-24.6	
65-70	Z	-35.5	
71-76	XCV	11.5[1]	Levels in XYZ System
77-82	YCV	18.1	
83-88	ZCV	114.6	
90-97	FLAG	00000001[2]	Level Flag
99-106	WORD 1	40000000[3]	State Vector
108-115	WORD 2	A51400A5	
117-124	WORD 3	50064D7F	

[1]Values greater than 2000.0 are flags.

[2]Unknown levels have a flag of 'FFFFFFFF' or 'EEEEEEEE'.

[3]Unknown states are set to zero.